DEPARTMENT OF THE AIR FORCE

HEADQUARTES, 603D REGIONAL SUPPORT GROUP (USAFE)

European Office of Aerospace Research and Development (EOARD)

Final Report of the Grant

Referring to

Grant # FA8655-06-1-3034

Performance 15 May 2006 to 15 May 2008

Title: **Discharge generation of atomic iodine for a COIL**

Investigators: Josef Schmiedberger, Vít Jirásek, Miroslav Čenský, Jarmila Kodymová, Irena Picková, Otomar Špalek

Contractor: Institute of Physics of Academy of Sciences CR
Dr. Jarmila Kodymová
Na Slovance 2
182 21 Prague 8
Czech Republic

Phone: +420 266 052 699
Fax: +420 286 890 265
E-mail: kodym@fzu.cz

Prime consultants: Dr. Timothy Madden
Dr. Kevin Hewett
USAF Research Laboratory /DED, Kirtland AFB, NM, USA

Date of report submission: 15 May 2008
24 months after the Grant award

REPORT DOCUMENTATION PAGE

Form Approved OMB No. 0704-0188

Public reporting burden for this collection of information is estimated to average 1 hour per response, including the time for reviewing instructions, searching existing data sources, gathering and maintaining the data needed, and completing and reviewing the collection of information. Send comments regarding this burden estimate or any other aspect of this collection of information, including suggestions for reducing the burden, to Department of Defense, Washington Headquarters Services, Directorate for Information Operations and Reports (0704-0188), 1215 Jefferson Davis Highway, Suite 1204, Arlington, VA 22202-4302. Respondents should be aware that notwithstanding any other provision of law, no person shall be subject to any penalty for failing to comply with a collection of information if it does not display a currently valid OMB control number.
PLEASE DO NOT RETURN YOUR FORM TO THE ABOVE ADDRESS.

1. REPORT DATE *(DD-MM-YYYY)*	2. REPORT TYPE	3. DATES COVERED *(From – To)*
27-05-2008	Final Report	15 May 2006 - 15-May-08

4. TITLE AND SUBTITLE

Discharge Generation of Atomic Iodine for a COIL

5a. CONTRACT NUMBER
FA8655-06-1-3034

5b. GRANT NUMBER

5c. PROGRAM ELEMENT NUMBER

6. AUTHOR(S)

Dr. Jarmila Kodymová

5d. PROJECT NUMBER

5d. TASK NUMBER

5e. WORK UNIT NUMBER

7. PERFORMING ORGANIZATION NAME(S) AND ADDRESS(ES)

Institute of Physics Academy of Science
Na Slovance 2
182 21 Prague 8
Czech Republic

8. PERFORMING ORGANIZATION REPORT NUMBER

N/A

9. SPONSORING/MONITORING AGENCY NAME(S) AND ADDRESS(ES)

EOARD
Unit 4515 BOX 14
APO AE 09421

10. SPONSOR/MONITOR'S ACRONYM(S)

11. SPONSOR/MONITOR'S REPORT NUMBER(S)
Grant 06-3034

12. DISTRIBUTION/AVAILABILITY STATEMENT

Approved for public release; distribution is unlimited.

13. SUPPLEMENTARY NOTES

14. ABSTRACT

This report results from a contract tasking Institute of Physics Academy of Science as follows: B. TECHNICAL PROPOSAL:
Tasks and objectives for 24 months
To conceptualize the problem based on the comprehensive literature study, theoretical estimation of particular problems, calculations, and elaboration of generator concept, including: estimations of advantages and disadvantages of considered precursors of atomic iodine(I2, CH3I, CF3I and HI, respectively); estimations of advantages and disadvantages of considered type of electric discharge(RF, MW, DC discharge), and discharge configuration employed; estimations of appropriateness of gases used for a discharge ignition and carrying gaseous ioidne precursors (Ar, He, N2, addition NO, NO2) from the point of reaction kinetics involved in the discharge plasma, heat capacity, etc.
To design a small-scale device to test experimentally the discharge I atom generation issuing from conclusions of the Task 1, including the following plans: The experiments will start with employing the RF discharge in a mixture of I donors (I2, RI) in a carrier gas due to a former experience with the RF discharge during research on the DOIL-related problems. The RF electrode discharge would be ignited directly inside the iodine injector in order to suppress iodine recombination to the lowest possible level. The RF iodine injector would be located in the center of supersonic nozzle throat.. This experimental configuration would allow testing all the above mentioned I precursors.
To suggest by CFD modelling, and experimental results of the Task 2 and chemically generated I atoms the most suitable configuration for mixing atomic iodine and O2(1D) flow.

15. SUBJECT TERMS

EOARD, Laser modeling, Chemical oxygen iodine lasers, Laser engineering

16. SECURITY CLASSIFICATION OF:			17. LIMITATION OF ABSTRACT	18, NUMBER OF PAGES	19a. NAME OF RESPONSIBLE PERSON
a. REPORT	b. ABSTRACT	c. THIS PAGE			A. GAVRIELIDES
UNCLAS	UNCLAS	UNCLAS	UL	44	19b. TELEPHONE NUMBER *(Include area code)* +44 (0)1895 616205

Contents

1. General outline of the grant

1.1. Outline of the grant subject and motivation

Atomic iodine for lasing of chemical oxygen-iodine laser (COIL) is generated by dissociation of molecular iodine by a process assisted with singlet oxygen ($O_2(^1\Delta)$) present in the laser medium. A theoretical estimate showed that energy of 4–10 $O_2(^1\Delta)$ molecules per one I_2 molecule is consumed in this conventional way, which could be otherwise utilized for laser gain and power increase.

Molecular iodine management involving evaporator and I_2 vapor transportation into a mixing region in the COIL through heated lines and injector represents quite complicated system, increasing a laser device weight.

A fast quenching of lasing species I^* by I_2 molecules (k = 3.1 x $10^{-11}cm^3molec^{-1}s^{-1}$) could be diminished by replacing I_2 with other iodine donor or atomic iodine generated directly in the COIL medium from gaseous reactants.

Atomic iodine generation from chemical reactants by the proposed chemical method via Cl or F atoms by their reaction with HI [1-5], has been characterized by a low efficiency due to an undesirable kinetic process in these reaction systems.

These arguments and published results on discharge generation of atomic iodine of other authors [6-14] discussed in details in the interim report of this grant [15] have motivated us to propose and investigate a discharge generation of atomic iodine from chosen iodine donor compounds eliminating a role of singlet oxygen in this process. A novel experimental configuration minimizing a recombination of generated I atoms before injection into the $O_2(^1\Delta)$ flow in COIL was also proposed.

1.2. Tasks for Research Periods 1 and 2 of this project

Period 1 (15 May 2006 – 14 May 2007)

- A conceptualization of the object of discharge generation of atomic iodine based on comprehensive literature survey, theoretical estimations of particular problems, calculations, and previous experiences in this field;
- A designing of the small-scale device supported with computational modeling of configurations and dimensions of the device components; elaboration of technical drawings for a device fabrication;
- Fabrication of individual parts of the device, purchasing of device accessories;

Detailed description of the research achievements during the Period 1 were presented in the submitted reports [15] and [16].

Period 2 (15 May 2007 – 15 May 2008)

- Finalizing of the construction of whole experimental device involving a gas-handling management, pressure and flow rates recording on-line, etc.;
- Starting with the device testing, first a cold-flow testing of the Mach number in the cavity with inserted originally designed supersonic nozzle/iodine injector body;
- Preparing a RF discharge measurements with suitable iodine donor compounds involving appropriate diagnostic techniques;
- Experimental investigations on atomic iodine generation from some donor substances (potentially CH_3I, CF_3I, C_3F_7I, I_2, HI) using the PSI Iodine Scan Diagnostics; evaluation of the atomic iodine yield related to initial donor concentration or a dissociation degree of RI molecules measured at different experimental conditions (RF discharge power, RF frequency, flow rates of iodine donors and buffer gas in the primary and secondary gases); mapping of atomic iodine concentrations recorded perpendicularly across the cavity;
- A suggestion of suitable configuration of the discharge generated atomic iodine mixing with the primary gas containing $O_2(^1\Delta)$.
- Performing a CFD modeling of the small-signal gain in the suggested device configuration for different degrees of predissociation of atomic iodine donor.

Detailed description of some fulfilled tasks of the Period 2 was presented in the submitted interim report [17].

2. Conception of the proposed method

A principle of the proposed method of discharge generation of atomic iodine for a COIL/DOIL is shown in **Fig. 1**. Our novel approach pivots on iodine atoms production directly in a specific shaped iodine injector forming the RF discharge chamber and simultaneously the supersonic double-slit nozzle. This injector/nozzle body inserted in the cavity center is profiled to choke the primary gas and expand the gas mixture to a supersonic velocity. The primary gas (N_2 or N_2/He mixture in a cold-flow testing or $O_2(^1\Delta)$/He mixture in a gain measurement) flows from a subsonic channel. A cross section of the subsonic channel 50mm × 9.5mm was determined to fit to the inlet cross-section of our laboratory COIL device.

The radio frequency discharge dissociates the iodine donor molecules introduced in a gas or vapor form in mixture with a buffer gas (He, Ar) into the iodine injector chamber. Discharge plasma is created from the gas mixture by means of the rod wolfram electrode inserted in the chamber center resulting in dissociation of iodine donor molecules. Atomic iodine generated in this way in the discharge medium can be immediately injected into the primary flow through the cavity.

Advantages of this original proposed concept should be following:

i) Heat dissipation into the primary flow in laser is diminished.
ii) A residence time of generated atomic iodine is very short.
iii) Recombination losses of generated iodine atoms before their mixing with $O_2(^1\Delta)$ are minimized.

iv) Injection of atomic iodine can be subsonic, transonic or supersonic. Homogenous recombination loss of I and I^*, and quenching by H_2O at the supersonic injection should be minimized.

v) Atomic iodine in the lasing upper state I^* can be also partially produced in the discharge cavity by the UV photolysis thanks to highly reflective aluminum wall of the injector (discharge) tube (a phenomenon well known from photodissociation iodine laser).

vi) A continuous or periodically pulsed mode of the RF device operation can be employed. A high electron density alongside a neutral low-temperature discharge species can be produced by the RF high-repetition rate operation. This should be beneficial for the iodine donor dissociation kinetics.

vii) Different iodine donors can be tested with this universal experimental configuration. Suitability of iodine donors for the COIL operation would be estimated from the operation ease given by donor physical and chemical properties, from the atomic iodine yield, discharge stability of the donor/carrier gas mixture, and also cost and commercial availability of donors.

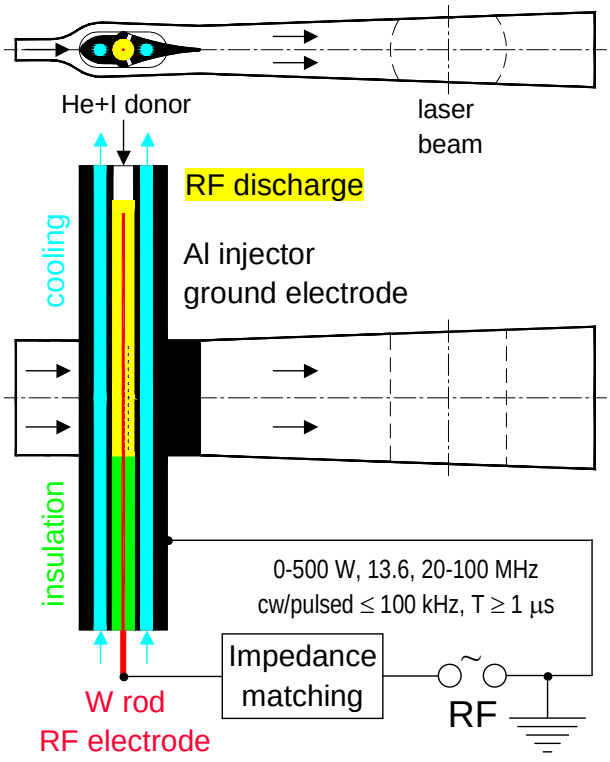

Fig.1. Principle of the RF discharge generation of atomic iodine

3. Device for discharge generation of atomic iodine (DAIG)

3.1. Design of main components and DAIG construction

The whole set of technical constructional drawings for DAIG device manufacturing was given in the reports of the Phases 1 of this grant [15] and [16]. The design and photos of some device components were shown in the interim report of the Phase 2 [17]. The most significant parts of the device, and some new parts finalized during this research term are reminded below in this report. **Figs. 2a,b** illustrate schematically a side and top view of the DAIG main body with the iodine injector/double slit supersonic nozzle.

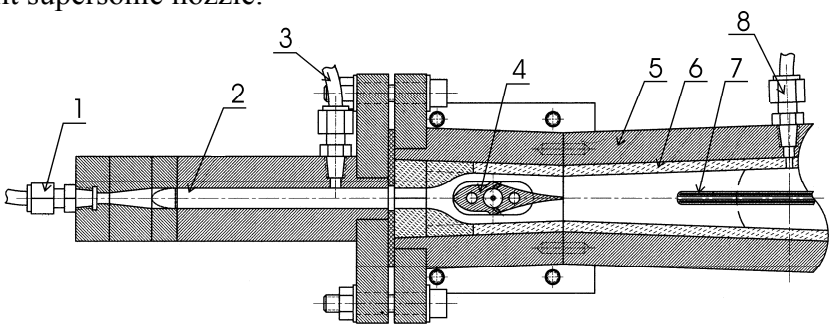

Fig.2a. Side view of DAIG device: 1 – inlet of primary gas flow; 2 – subsonic duct; 3 – pressure detection in subsonic duct; 4 – iodine injector/double slit supersonic nozzle; 5 – Plexiglas supersonic cavity; 6 – thin pane; 7 – Pitot tube; 8 – pressure detection in supersonic cavity

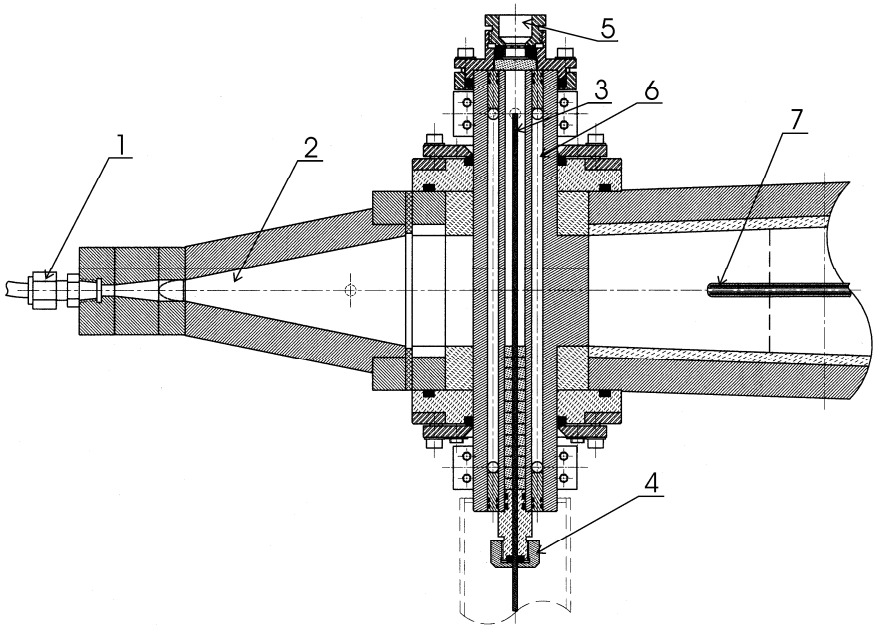

Fig.2b. Top view of DAIG device: 1 – inlet of primary gas flow; 2 – subsonic duct; 3 – RF tungsten electrode; 4 – RF input sealing nut; 5 – optical window flange for discharge observation; 6 – tubes for cooling/heating medium; 7 – Pitot tube in supersonic cavity

The RF discharge cavity, iodine injector, and double slit supersonic nozzle in one body (4 in Fig.2a) is a crucial component of the device, shown in the constructional details in **Fig. 3.**

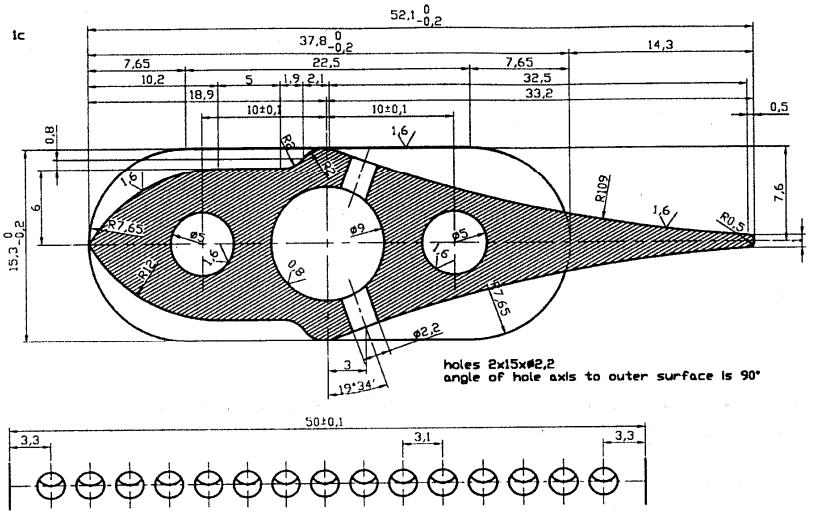

Fig.3. Body of RF discharge cavity (middle hole), iodine injector, and double-slit nozzle

A shape of this body and its dimensions were designed by means of the 2-D method of characteristics, 1-D isentropic flow calculations and CFD modeling [18]. The Mach number 2 was supposed in the expansion region for the primary gas flow composed of O_2/He mixture (1:2, κ = 1.547), corresponding to the jet SOG operation in our COIL device. Contours of the Mach number of gas flow along the body are shown in **Fig. 4,** obtained by 2-D numerical simulation

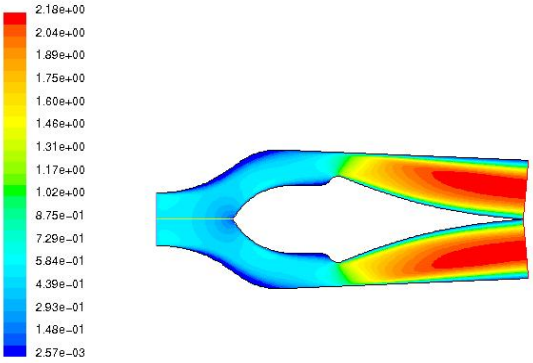

Fig. 4 b. Mach number in vicinity of the injector body; 2D simulation

Details of these calculations were presented in the report of this grant [16]. The calculations counted with the expansion ratio $A_{\exp} / A_{throat} = 2.5$, the nozzle throat width 50 mm, and the vacuum pumping system of nominal capacity Q = 3000 m^3/h. The optimal throat height 4 mm of one slit of the double-slit nozzle was calculated. The body of fabricated injector/supersonic nozzle is shown in **Photo 1**.

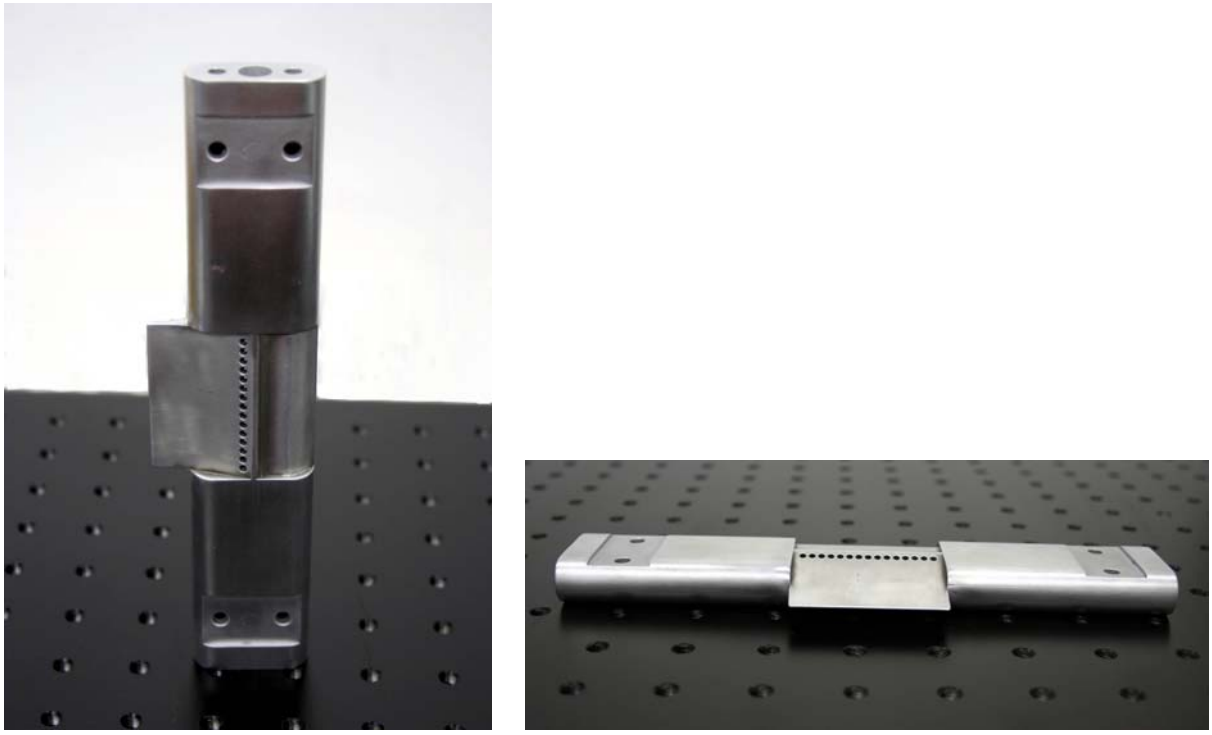

Photo 1. Iodine injector/supersonic nozzle (middle part of body)

The injector is made of pure aluminum (99.5% Al, A1050). This material is highly resistant to corrosion of iodine, very good electrically and thermally conductive, and little efficient to singlet oxygen quenching (like a glass). A middle channel of inner diameter 9 mm forms the discharge chamber and its body is the ground electrode of the RF discharge. Axially inserted RF wolfram electrode has 2 mm in the outer diameter. Both electrodes are in the coaxial arrangement separated by heat-resistant glass rings on the side of RF input. The injector/chamber is directly connected to the impedance matching box. The carrier gas (mixture of He and Ar) and the iodine donor (CH_3I or CF_3I) are fed into the discharge chamber from the opposite side. The left and right holes (channels) of inner diameter 5 mm serve for introducing either cooling or heating medium (ethanol or water), depending on the iodine donor, which enables to keep a temperature of the discharge cavity in the range of 230–360 K.

The injector orifices were designed also by means of non-dimensional penetration parameter correlations and 3-D modeling of the atomic iodine homogeneity in the supersonic cavity. Details of these calculations and resulted parameters for several injectors were given in the reports [16] and [17]. The parameters of the injector employed in the experimental investigation performed in this research period are summarized in **Table 1**. This injector is suitable for a supersonic injection and lower flow rates.

A mixing chamber for fast mixing of the carrier gas (mixture of Ar and He) and the iodine donor (CH_3I or CF_3I) was designed as a small stainless steel cylindrical vessel of inner volume of ~1.1 cm^3 with three gas ports and one window. Two inlet ports introduced the carrier gas and the

iodine donor, both were introduced tangentially through the cylinder wall to form a vortex mixing. The third outlet port at the bottom of the vessel led the mixed gas directly to the discharge chamber at the RF electrode tip side. The top of the vessel was closed by the optical window to observe possibly the electrode tip. This mixing chamber is shown in the technical drawing in **Fig. 5** and can be also seen in **Photo 6** (No 3).

Tab. 1

Designed parameters of iodine injector used in experiments

N – number of holes in one row on one injector side; *n* – total molar flow rate (through upper and bottom row); *D* – hole diameter; p_{sec} – total pressure in injector; $y_r(4D)$ – relative penetration depth at distance of 4 orifice diameters

Injector type	n_{prim}, mmol/s	n_{sec}, mmol/s	D, mm	N	α, deg	area, mm^2	p_{sec}, Pa	q	$y_r(4D)$
1c	60	8	2.20	15	90	57.02	1881	3.08	0.24

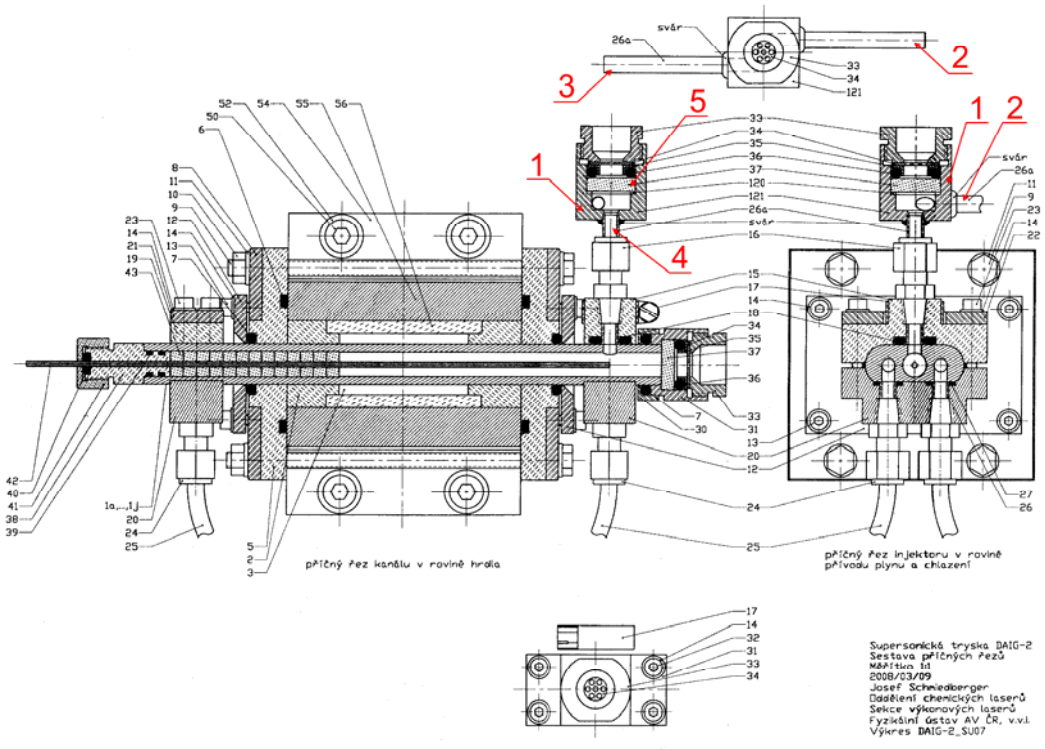

Fig. 5. Technical drawing of top view of DAIG device with details of secondary gas mixing chamber
1 – mixing chamber, 2 – iodine donor inlet, 3 – carrier gas inlet, 4 – gas mixture outlet, 5 – optical window

During the last research period of this grant (6 months), much time and effort was devoted yet to completion of the whole DAIG experimental system. These activities concerned mainly:

i) Iodine donor handling and preparing for experiments
ii) Gas handling system (e.g. replacing gas pipes of ¼" for 3/8" and shortening them to be able to get higher flow rates)
iii) Gas mixing (manufacturing the mixing chamber)
iv) Water cooling/heating line for injector and RF power source cooling
v) Iodine trap cooling (installation and testing of new cooler/heat exchanger)
vi) Iodine trap washing/draining (installation of glass tank for chemical solution and water)
vii) RF power connection and impedance matching (testing the RF discharge source operation)

The small-scale device constructed for performing the research on the discharge generation of atomic iodine is documented by the **Photos 2–19**.

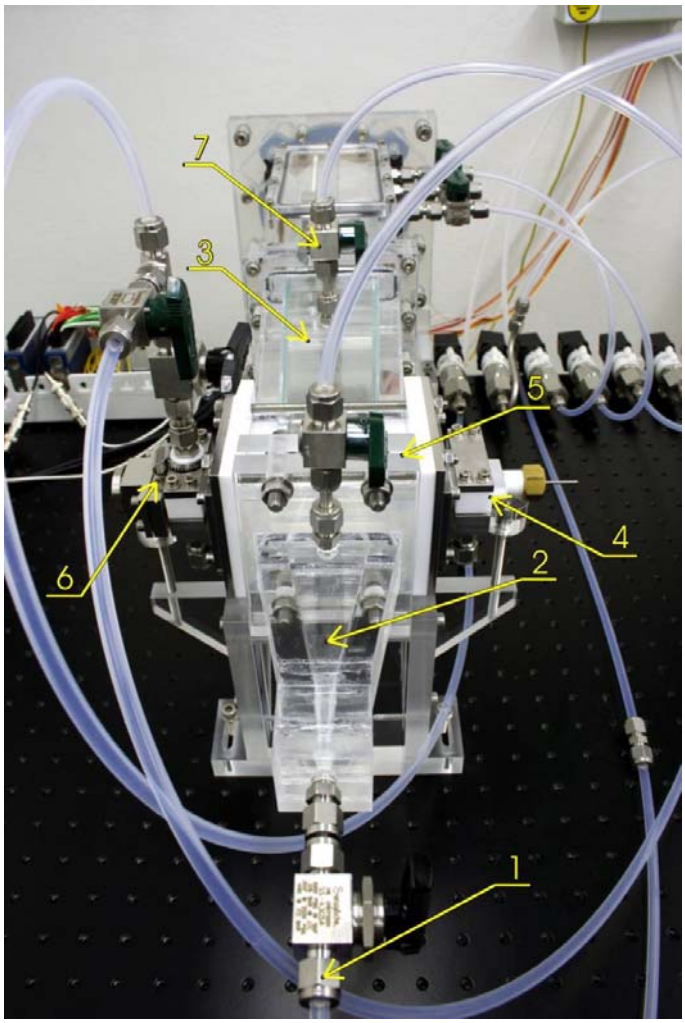

Photo 2. Main part of device from the front view
1 – inlet valve of primary gas
2 – subsonic expansion delta
3 – supersonic cavity with inserted iodine injector/double slit nozzle body
4 – RF power input with inserted electrode
5 – location of injector/double slit nozzle body
6 – arm with input of iodine donor/carrier gas mixture
7 – valve for pressure measurement in the expansion cavity

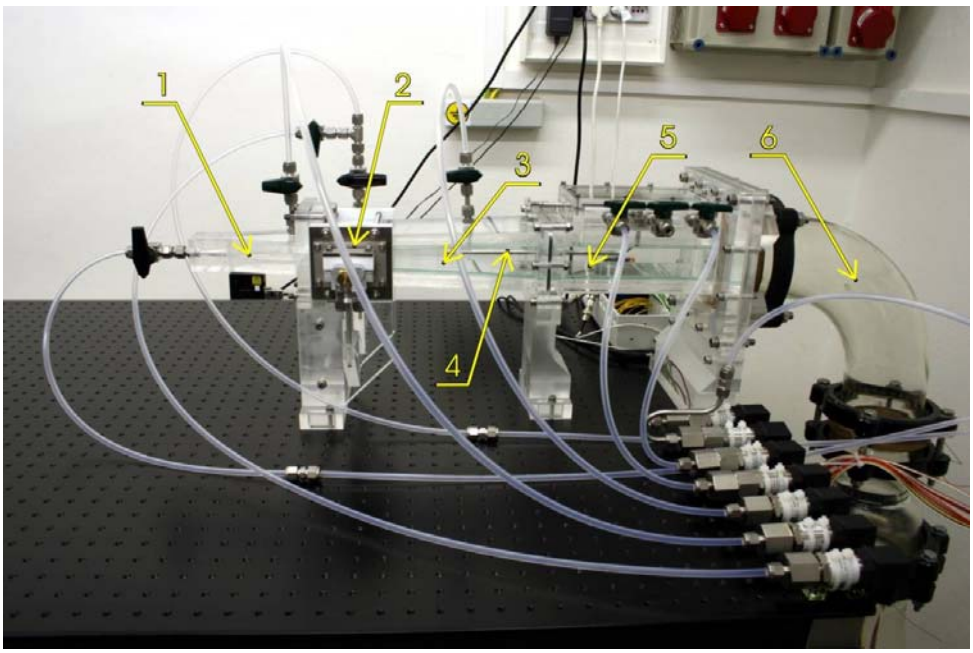

Photo 3. Device from the side view
1 – delta inlet of primary gas, 2 – thermally and electrically insulating bed for iodine injector/double slit nozzle, 3 – supersonic expansion cavity, 4 – movable Pitot tube, 5 – diffuser duct,
6 – Simax glass elbow tube connected with I_2 trap

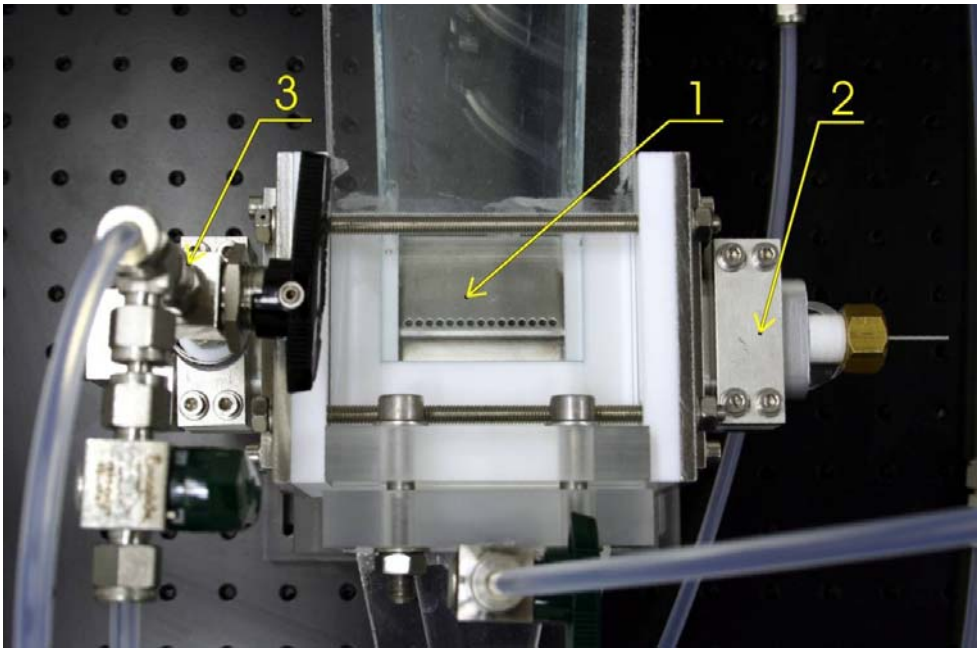

Photo 4. Top view on iodine injector / double slit nozzle
1 – middle part of injector/nozzle body, 2 – RF power input of wolfram rod electrode
3 – iodine donor inlet side of injector

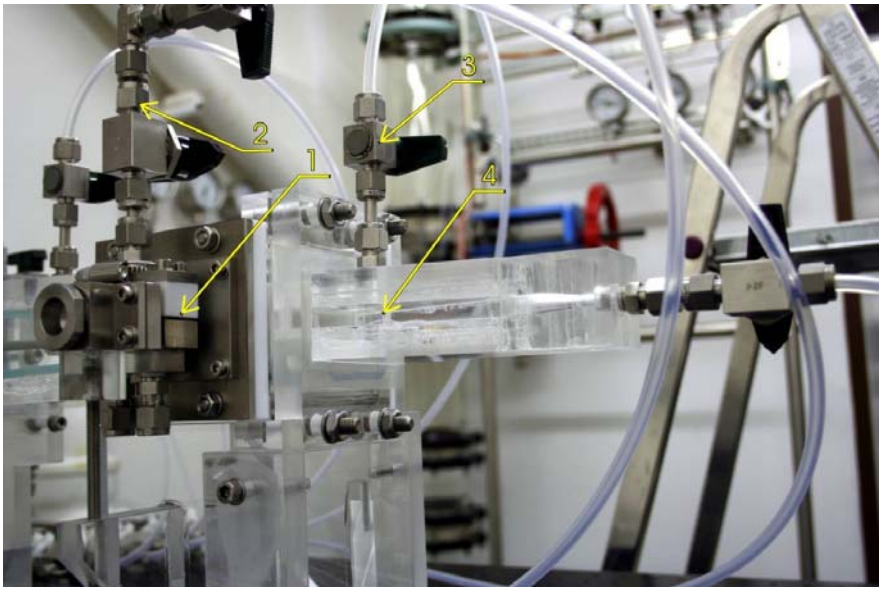

Photo 5. Device details
1 – flange of iodine donor/carrier gas mixture inlet, 2 – shut valve for iodine donor carrier gas input, 3 – valve for primary gas pressure measurements, 4 – subsonic delta cavity

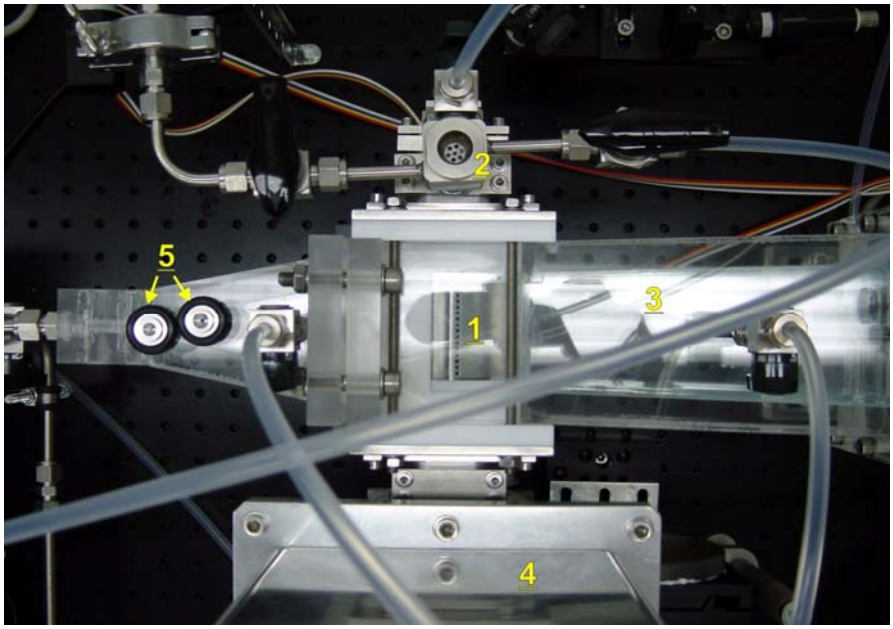

Photo 6. Device details
1 – injector/double slit nozzle, 2 – mixing chamber of iodine donor with carrier gas,
3 – supersonic cavity, 4 – RF discharge impedance, 5 – flow rate measuring diaphragms

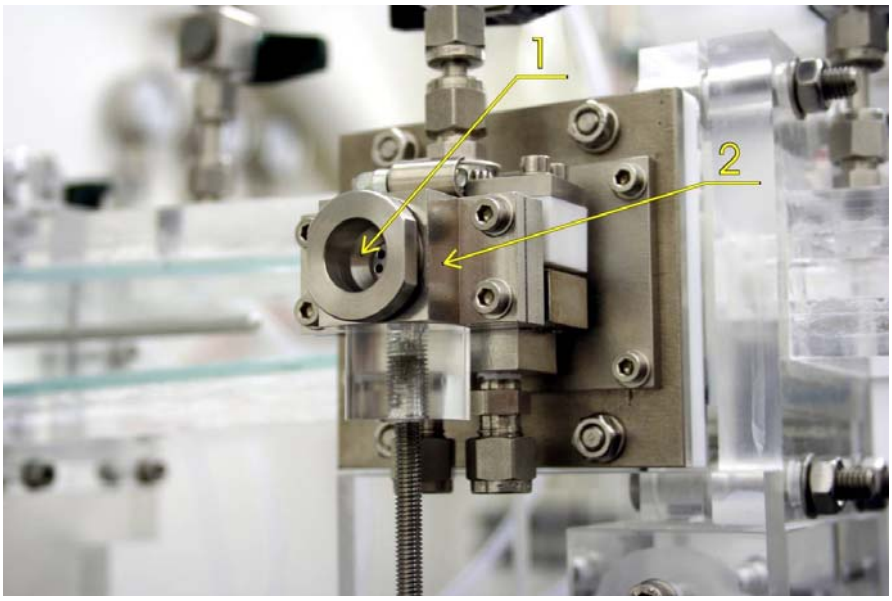

Photo 7. Device details
1 – diagnostic and observation window of discharge chamber with RF shielding mask,
2 – flange of diagnostic and observation window

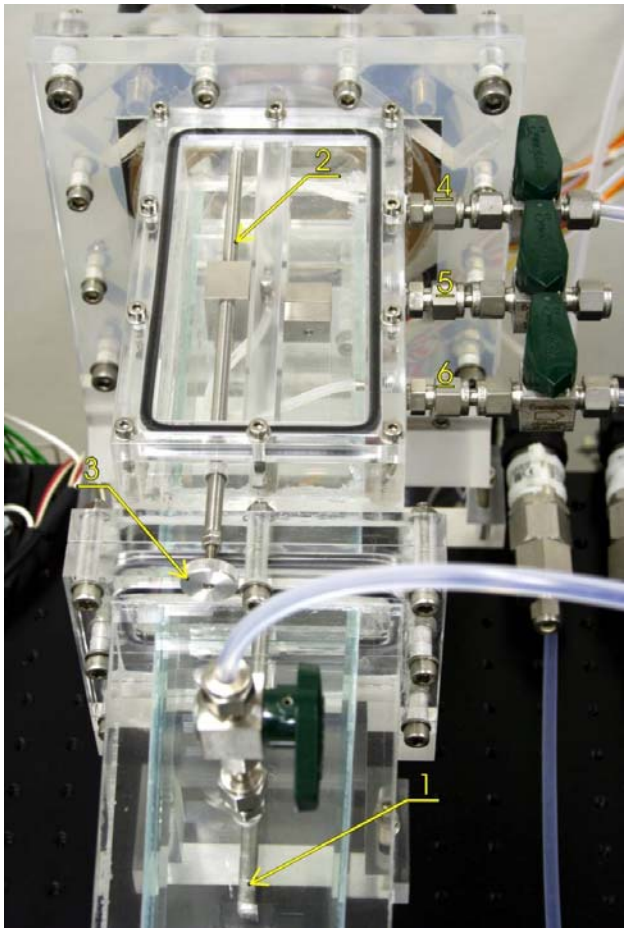

Photo 8. Device details
1 – movable Pitot double-jacketed tube
2 – screw thread rod for Pitot tube positioning along downflow duct axis
3 – hand wheel for screw thread rod
4 – pressure measurement port with shut valve for recording dynamic Pitot tube pressure
5 – pressure measurement port with shut valve for recording diffuser pressure
6 - pressure measurement port with shut valve for recording static Pitot tube pressure

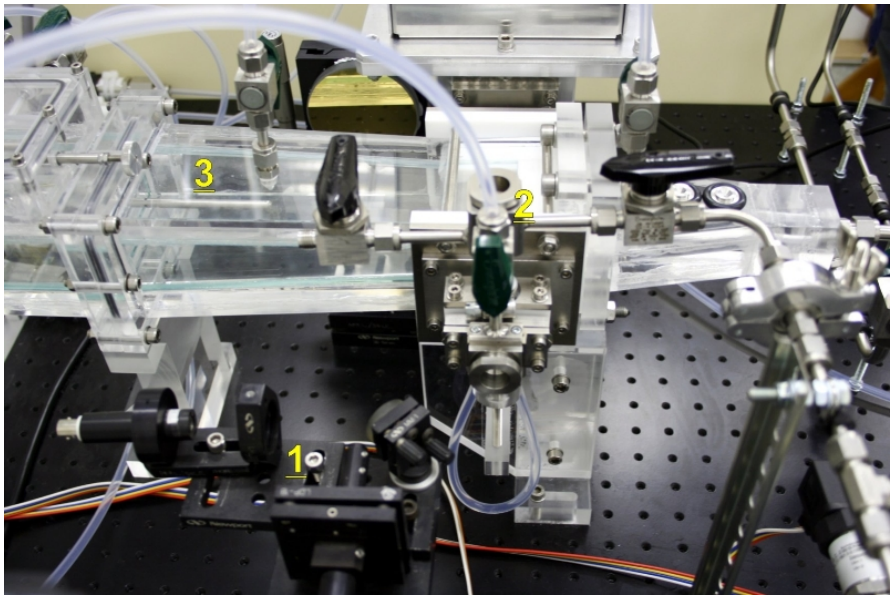

Photo 9. Device details
1 – Iodine Scan Diagnostics on moving stage, 2 – inlet of RI/carrier gas mixture, 3 – supersonic cavity

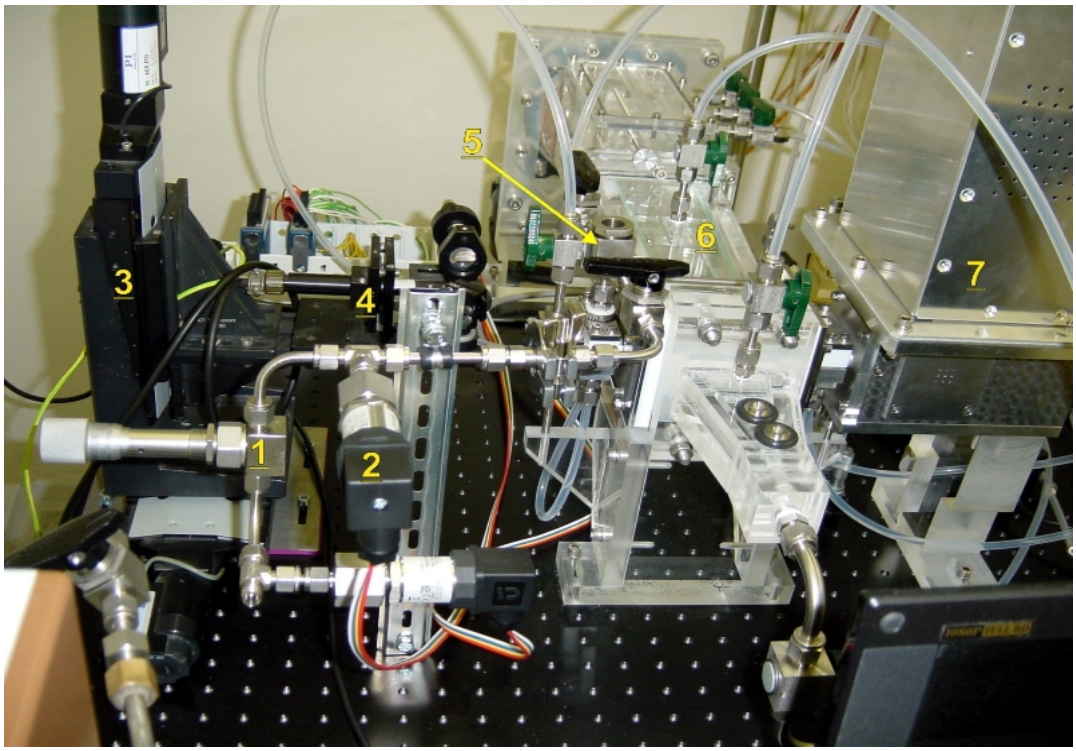

Photo 10. View on the whole device and measuring techniques
1 – needle valve for adjusting of iodine donor flow rate, 2 – pressure gauge, 3 – moving stage for ISD diagnostics, 4 – ISD probe, 5 – mixing chamber for inlet of iodine donor and carrier gas, 6 – region for atomic iodine detection (supersonic cavity), 7 – impedance matching box

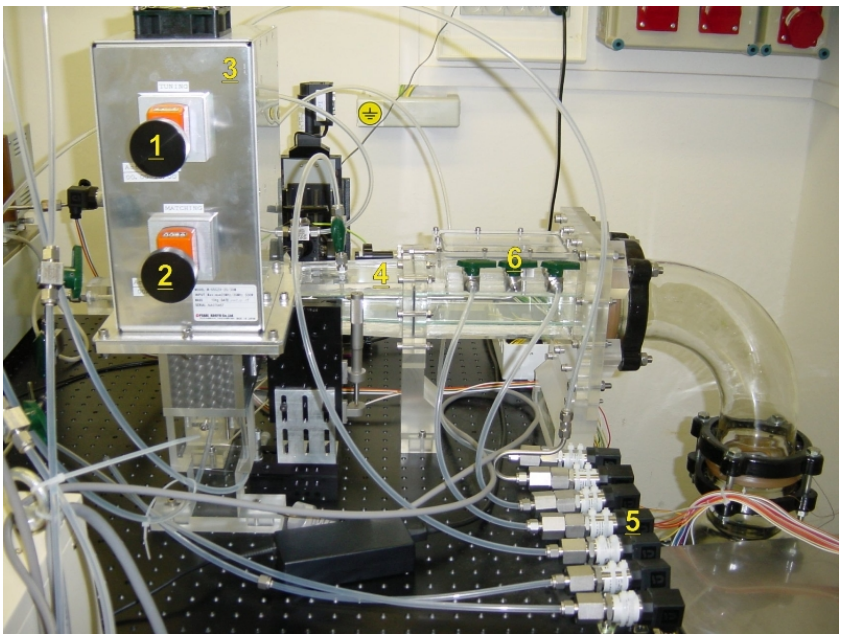

Photo 11. Device details
1 – RF impedance tuning knob
2 – RF impedance matching knob
3 – Impedance matching box
4 – cavity for atomic iodine detection
5 – set of pressure transducers
6 – Pitot pressure detection

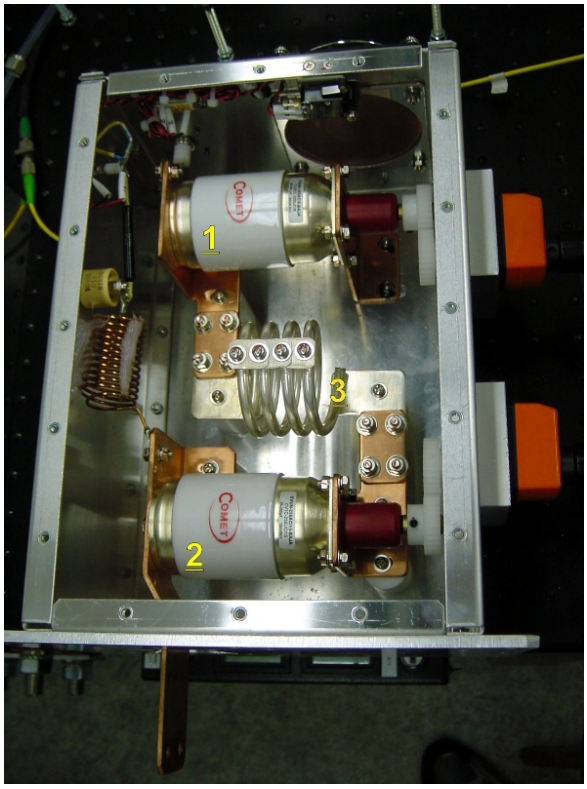

Photo 12. Inside view of impedance matching box
1 – variable capacitor of impedance tuning
2 – variable capacitor of impedance matching
3 – impedance matching coil

Photo 13. RF discharge source (details in text)

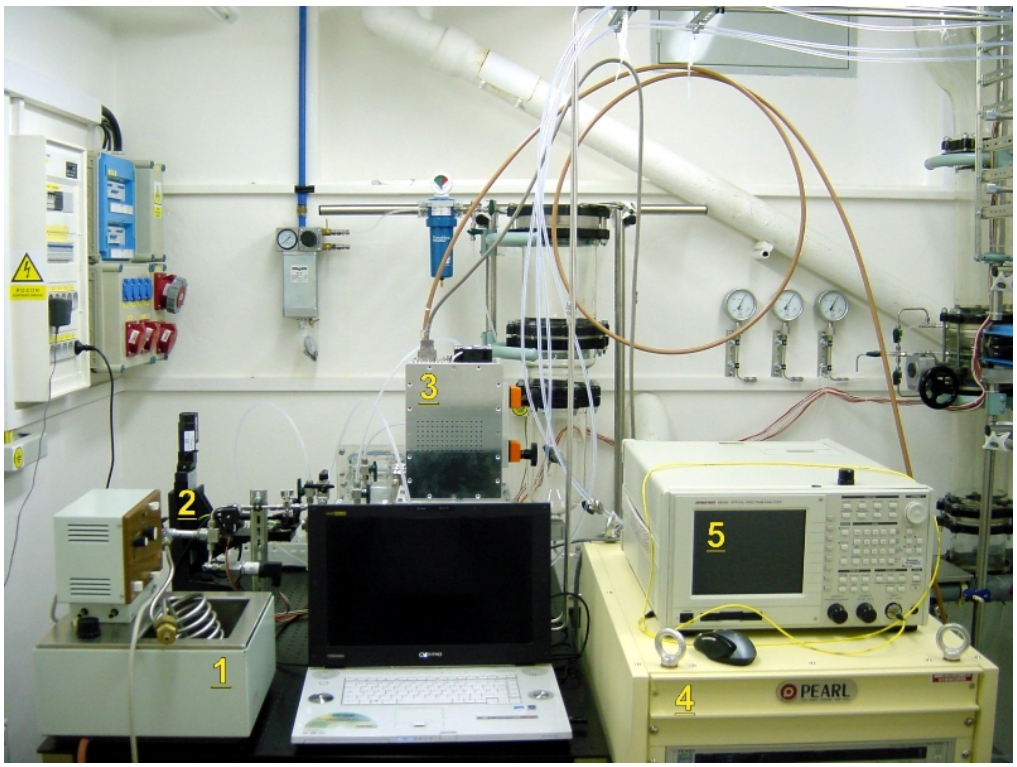

Photo 14. Overall device set-up
1 – thermostat for heating of iodine donor reservoir, 2 – Iodine Scan Diagnostics on moving stage,
3 – RF impedance matching box, 4 – RF source, 5 – optical spectral analyzer
Double pass ISD configuration shown here was changed to single pass after first experiment –see chapter 3.2

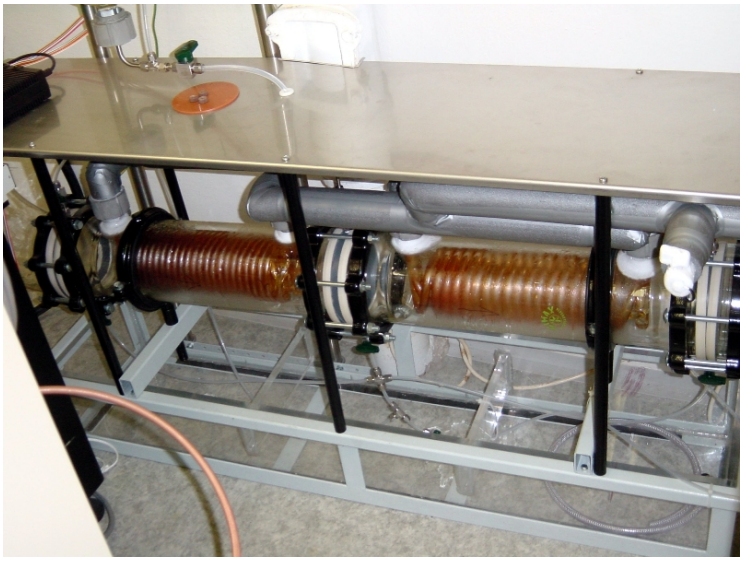

Photo 15. Spiral condenser iodine trap
(after experimental run with I_2 trapped from CH_3I)

Photo 16. Glass tank for sodium thiosulphate solution or water for trap cleaning

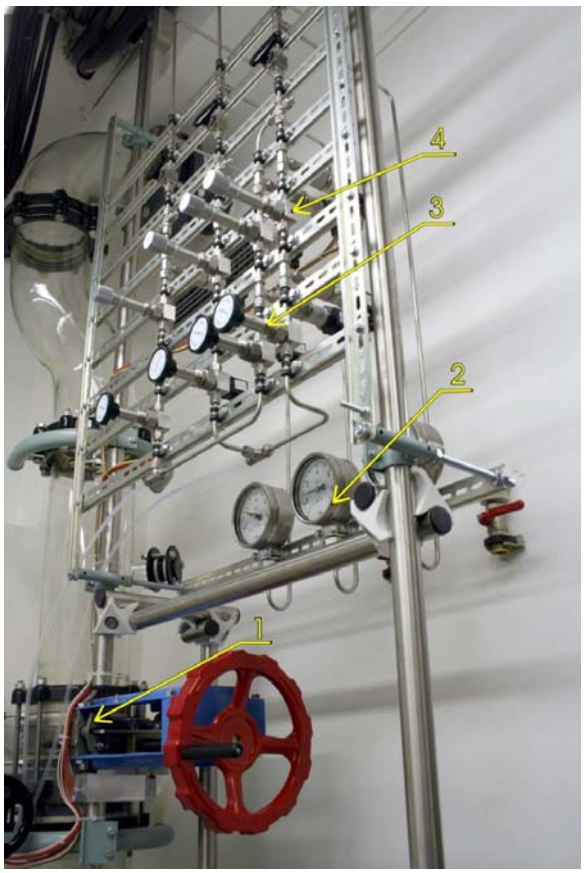

Photo 17. Device details
1 – vacuum shut slide and throttling butterfly valve
2 – pressure meters
3 – control needle valves
4 – measuring needle valves

Photo 19. Cooling unit for ethanol cooling in trap

3.2. DAIG device description and operation

Detail description of the device and diameters of individual parts were presented in the reports [16] and [17]. Here is given essential information only for reminding. Whole DAIG device body was made of optically transparent Plexiglas, which is suitable for optical measurements of iodine and gain via the cavity walls, enabling determination of optimal distance of resonator axis from atomic iodine injection for later laser experiments, and also for easy observation of discharge "flames" in the vicinity of the injector holes. Inner Plexiglas surface was protected from a heat released in the reaction medium with a thin pane. A movable Pitot double-jacketed tube is inserted in the cavity center, and can be movable along the gas stream during experimental run without disassembling the device.

Gas handling system

A gas handling system is formed by three gas lines, for He (99.996%), Ar (99.998%), and N_2 (99.998%). Each gas line consists of a gas pressure cylinder with pressure regulation valve (placed in a box outside), gas pipeline feeding the gas to the laboratory, flow meters, and gas mixing. The helium pipeline is split into two arms for using He as a primary and secondary gas. Flow meters consist of a needle valve and two pressure transducers measuring the pressure upstream and downstream of this valve. The needle valve with micrometer setting enables to change accurately a pressure drop in the range of several orders of magnitude, and thus to measure a flow rate in very wide range. Such flexible tool employed for the flow measurements is not commercially available. The new flow meters were calibrated by means of two commercial mass flow-meters. Details of this procedure were described in the report [17].

Alkyliodides CH_3I and CF_3I purchased from the Sigma Aldrich Ltd. were used as the iodine donors during this research period. **Table 2** contains their characteristics and physical properties.

Tab. 2
Characteristics and physical properties of tested iodine donor CH_3I and CF_3I

	CH_3I, Methyl Iodide (Iodomethan)	**CF_3I,** Trifluormethyl Iodide (Trifluoroiodomethan)
Molecular weight	141.95 g/mol	195.91 g/mol
Appearance	Colorless transparent liquid	
Density (specific gravity)	2.28 g/ml	2.36 g/ml
Solubility in water	slightly soluble (1.4 g/100 g at 20°C)	
Solubility in organic solvents	Readily soluble in alcohol, ether	
Melting point	-66.45 °C (206.7 K)	
Boiling point	42.55 °C (315.6 K)	-22.5 °C
Viscosity of liquid	0.594 mPa s at 0°C 0.469 mPa s at 25°C	
Refractive index	$n^{21}{}_D$ 1.5293	
Vapor pressure, kPa	1 (-49°C), 10 (-12.4°C), 100 (42°C)	
Thermodynamic properties	ΔH_o (liq) = -13.6 kJ/mol ΔH_o (gas) = 14.4 kJ/mol C_p (liq) = 126.0 J/mol K C_p (gas) = 44.1 J/mol K	-587.8 kJ/mol 70.9 J/mol K
Enthalpy of vaporization of liquid	ΔH_{vap} (t_{bp}) = 27.34 kJ/mol ΔH_{vap} (25°C) = 27.97 kJ/mol	
UV photonic quantum yield	$f^* = [I^*]/[I^*] + [I] \sim 0.92 \pm 0.02$	$f^* = [I^*]/[I^*] + [I] \sim 0.91 \pm 0.03$
Collisional deactivation	$I^* + CH_3I \rightarrow I + RI$ $k = 2.6 \times 10^{-13}$ cm^3 molec^{-1} s^{-1}	$I^* + CF_3I \rightarrow I + RI$ $k = 3.5 \times 10^{-16}$ cm^{3}molec^{-1}s^{-1}
Reaction (possible at DIG)	$CH_3 + O \rightarrow$ product $k = 1.1 \times 10^{-10}$ (T = 298 K)	
Hazard properties	non-inflammable, non-explosive	

The CH_3I liquid was kept in a closed cylindrical stainless steel vessel preventing it from decomposition by light. Before experiments, the vessel was immersed in warm water of the thermostat with temperature of ~40°C–50°C to achieve a higher saturated vapor pressure of alkyliodide, needed for higher flow rates of the donor. A maximum flow rate of 0.77 mmol/s was attainable at 48°C corresponding to a vapor pressure of 107 kPa. At the temperature higher than 50°C a slight condensation of the donor already started on stainless steel pipe walls connecting the vessel with the device. A flow rate of the iodine donor was measured by means of pressure measuring before the diaphragm (sonic orifice). The flow rate was calibrated by means of Ar and then recalculated for the molecule of CH_3I.

The CF_3I donor had a sufficient vapor pressure at room temperature, which conveniently allowed using it directly from the commercial pressure container equipped with a pressure regulating valve. The flow rate was measured in the same way as in the case of CH_3I.

Pressure measurement

Pressure in several important points of the DAIG device was measured by electric pressure transducers of strain gauge type (for a pressure range 0-10 kPa, 0-25 kPa, and 0-100 kPa). The USB Data Acquisition System of the National Instruments Comp. (type NI cDAQ-9172 with module NI 9205) recorded signals of 0-10 V from all pressure transducers, and data were processed by PC on-line with a developed program under the LabView software. Before starting the experiments with iodine donors, all transducers were calibrated in the pressure range of 50–1000 Pa by means of a precise capacitive pressure gauge (Leybold Ltd.). A pressure in the cavity during experiments was measured as a standard static wall-pressure at 140 mm downstream the nozzle throat. A tip of the Pitot tube was 155 mm downstream the nozzle throat.

Discharge chamber

The discharge chamber with inserted wolfram rod RF electrode was water-cooled (10°C) during all experimental runs with atomic iodine generation. This chamber was a part of the iodine injector (see Fig. 1-3 and Photo 1) that had relatively large holes (2.2 mm i.d.) in the first experimental sets performed during this research period. This was chosen for the reason to avoid atomic iodine recombination on the holes but it had some disadvantage from the point of discharge generation, as shown only during experiments. This configuration caused a pressure drop along the row of injecting holes with the lowest pressure on the opposite side of the gas introducing (the end of the discharge chamber with the glass insulation). This resulted in a carbon deposit from the decomposed iodine donor.

RF power source

The RF power source used in below described experiments was a wideband tunable cw/pulse radiofrequency generator of the following specification and parameters:

- producer PEARL KOGYO Co., Ltd, Osaka, Japan
- model CF-500-20/100M
- oscillating frequency 20-100 MHz

- output power ≤ 500 W
- output impedance 50-52 Ω for unbalanced load
- mode of operation cw/pulsed
- pulse frequency 100 Hz – 99 kHz
- minimum pulse length < 2 μs
- pulse duty ratio 5-95 %
- pulse rise time < 1.0 μs
- displayed parameters forward power, reflected power, VDC voltage

Impedance matching network

The RF output power is fed into the discharge by means of the L-type impedance matching circuit connected to the power source by a coaxial cable. The electric scheme of the matching network is in **Fig. 6.**

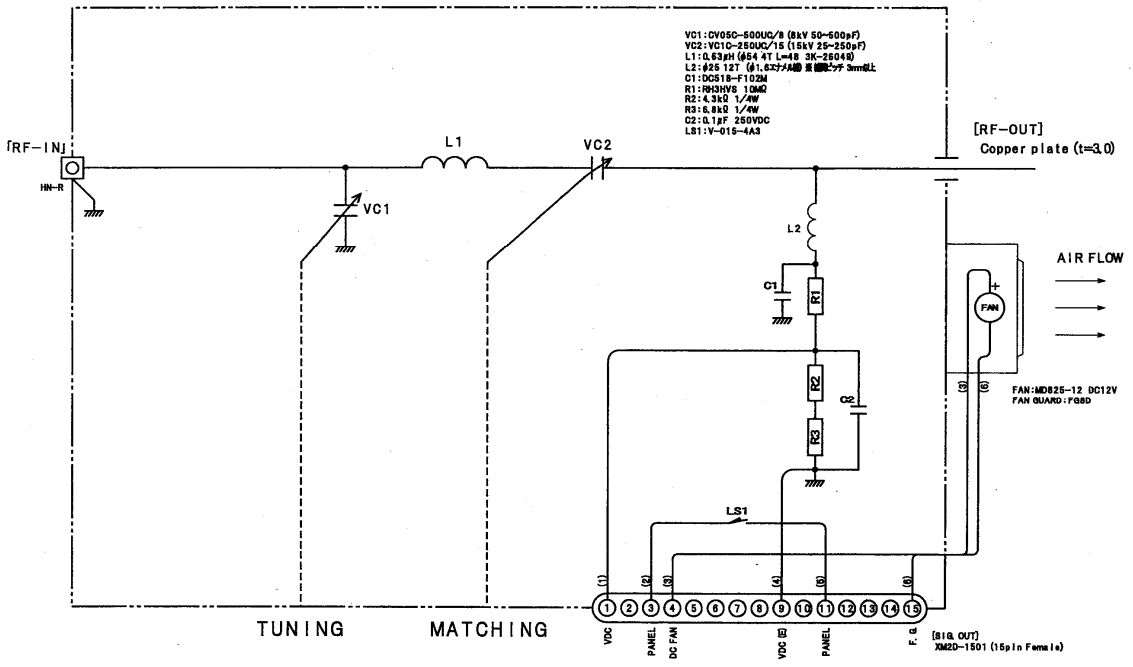

Fig. 6. Electric scheme of impedance matching circuit for 30-60 MHz frequency range

The impedance matching circuit is arranged in a grounded shielding box, attached directly to the discharge chamber to ensure the shortest distance between the load and matching box and thus the best impedance matching. There are 3 different matching boxes for 3 different frequency domains; 20-30 MHz, 30-60 MHz and 60-100 MHz. The scheme in Fig. 6 is relevant to 30-60 MHz. The other matching boxes have basically the same scheme with different values of capacity of variable

capacitors and different values of inductance of the RF matching coil. The parameters are given in **Table 3.** The matching coil can be changed by short connection of adjacent turns (decreasing the inductance by several steps).

Tab. 3
Parameters of matching box of RF power source

Frequency range	VC1 tuning	VC2 matching	L1 matching
20-30 MHz	100-1000 pF	50-500 pF	0.85 μH (ø = 54 mm, 5 turns, L = 60 mm)
30-60 MHz	50-500 pF	25-250 pF	0.63 μH (ø = 54 mm, 4 turns, L = 48 mm)
60-100 MHz	25-250 pF	10-100 pF	none

The impedance matching box connected with RF rod electrode is in details shown in the technical drawing in **Fig. 7.**

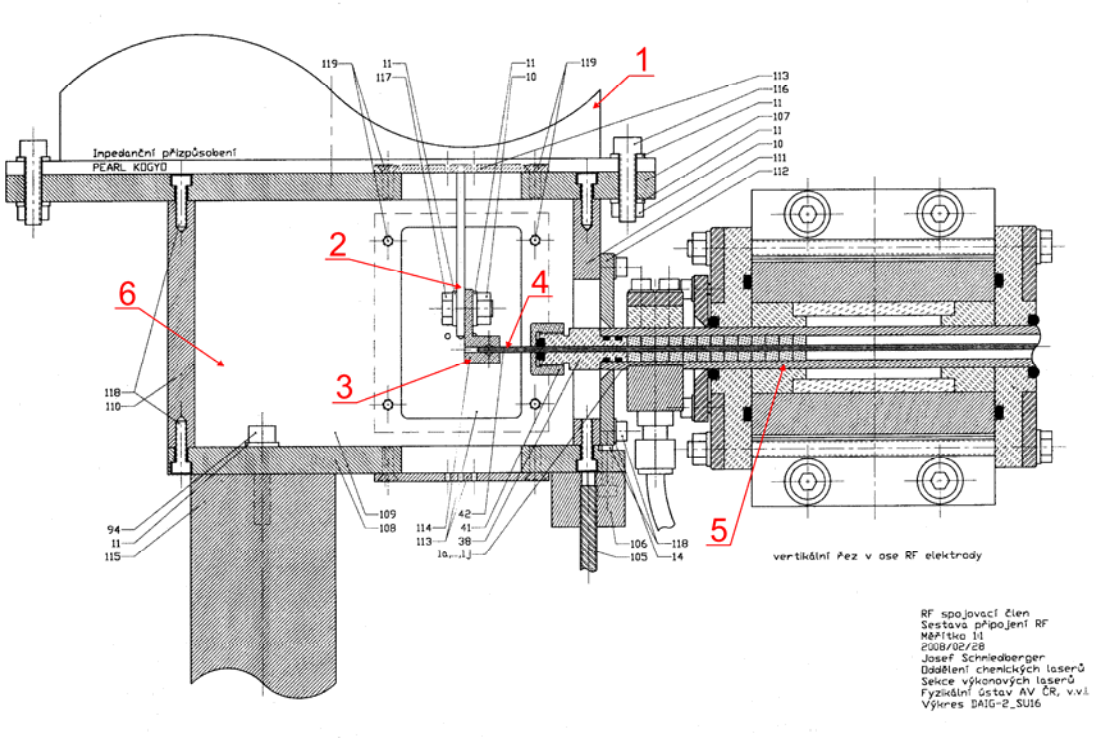

Fig. 7. Details of RF power source connection with discharge chamber
1 – impedance matching box, 2 – copper strip RF output; 3 – copper connector,
4 – RF W electrode, 5 – Al injector (discharge chamber), 6 – connecting chamber

The initial tests were done at the radio-frequencies of 20 and 30 MHz, which however showed that the impedance matching was not good. The minimum capacity of VC1 (100 pF) and VC2 (50 pF) was too high for any inductance L1 ≤ 0.85 μH, resulting in the reflected RF power ~55% of the forward RF power. This limited the first tests to a range of the small power ($P_{forward} \leq 100$ W,

$P_{reflected} \leq 55$ W). A perfect impedance matching was achieved at 40 MHz, when the matching box parameters were set as follows: VC1 ~ 95 pF, VC2 ~ 47.5 pF and L1 = 0.63 μH. A variation of these optimum values due to any change in the gas mixture composition and pressure in the discharge chamber was tiny, amounting to a few percent. A degree of the impedance matching can be illustrated by a typical example: $P_{forward}$ = 250 W, $P_{reflected}$ = 2 W, $P_{reflected}/ P_{forward}$ = 0.8 %.

RF discharge performance

All further discharge experiments were performed at the radiofrequency of 40 MHz exhibiting an excellent impedance matching. First tests of the burned discharge were with the Ar+He mixture without the iodine donor, and a violet-blue flowing afterglow could be visible outside the injecting holes. These flames were ~5-10 mm long, and were longer on the lower pressure end in the injector and shorter on the higher pressure end (see above mentioned a pressure drop inside). This qualitatively proved that a higher plasma density can be expected at the lower pressure in the discharge chamber. An example of such flames can be seen in **Photo 20.**

Photo 20. Discharge afterglow flames of Ar+He mixture plasma in vicinity of iodine injector holes

When the iodine donor was added to the carrier gas (He, Ar), the flowing afterglow flames disappeared, the discharge color changed in violet-white, and the impedance matching had to be dramatically changed. This was caused by the strong electro-negativity of the iodine donor.

Molecular iodine trap

Spiral condensers made of Pyrex industrial chemical glassware (see Photo 15) were used for trapping residual gases (mainly recombined I_2 vapor) exiting the device diffuser. To estimate an efficiency of I_2 vapor capturing, a theoretical estimation was performed based on a heat transfer coefficient and friction coefficient and using the Reynolds, Nusselt and Prandtl numbers [19]. A detail mathematical apparatus for these calculations were presented in the report of this grant [15]. The results of these estimations are repeated in **Table 4**.

Tab. 4
Input data and calculation results for the iodine trap

Gas pressure	600 Pa = 4.5 Torr	Viscosity	2.03 e-5 Pa.s
Gas temperature	320 K	Heat capacity	2085 J/kg/K
Composition (mmol/s)	$He:O_2:I_2$ = 120:40:0.5	Heat conductivity	6.28 e-2 W/m/K
Heat exchange area of one condenser unit	0.75 m^2	Heat transfer coefficient	29 $W/m^2/K$
Length of one condenser unit	0.3 m	Gas velocity	80.6 m/s
Free stream area	88 cm^2	Reynolds number	148
Minimum trap length	0.6 m	Pressure loss	150 Pa
Minimum cooling power	245-318 W by the cooling medium temperature		

The trap consists of two spiral condensers of the inner diameter of 150 mm, and the active length of one unit is about 30 cm. Ethanol is used as a coolant medium. A 3°-slope makes easier a cleaning maintenance without disassembly and reassembly after finishing the experiments. A heat exchanger for ethanol cooling in this condenser was designed and fabricated by the commercial Czech company (Horkan Klima, Ltd., Czech Republic) having a cooling power of 2.2 kW at -45°C to -32°C (see Photo 19). The spiral condensers were cooled by ethanol circulating by means of the pump (Grundfos Comp.) between the iodine trap and cooling unit (heat exchanger). A circulating ethanol volume is about 10 liters. The operation temperature up to -35°C was achieved within 35 minutes.

After experiments the vacuum duct with the spiral condensers was filled with ~40 l of warm water solution of sodium thiosulphate (~40°C) at atmospheric pressure. The solution was prepared in a separate glass tank (see Photo 16). All trapped I_2 and probably other undefined deposits (e.g. RI, R-R) on the glass surface were dissolved in this solution within few minutes. The waste solution was drained by a water pump. This procedure was then repeated twice with warm water only to remove remaining impurities. Remaining water moisture was dried by evaporation by vacuum. This procedure enabled to clean the trap completely without disassembly of the vacuum system.

The vacuum complex consisting of the rotary and Roots pumps (total capacity ~3000 m^3/h) was used for the gas exhausting through the vacuum tube of inner diameter 150 mm involving a shut slide valve and throttling butterfly valve.

Iodine Scan Diagnostics

PSI Iodine Scan Diagnostics (ISD) based on a narrow band tunable diode probe laser was used for evaluation of atomic iodine concentrations and temperature in the cavity by measuring absorption for the $I(^2P_{1/2})$ - $I(^2P_{3/2})$ transition at 1315 nm. The ISD probe beam emitter/detector unit was mounted on the assembly of motorized linear positioning equipment controlled by PC. Concentration profiles of atomic iodine across the expansion cavity perpendicularly to the gas flow were recorded at distances between 87.2 to 188.2 mm from the nozzle throat. Absorption length in this range changed from 54 to 58 mm. A probe beam was moved in the vertical direction with the velocity of 2 mm s^{-1}. A single-pass configuration of the ISD beam was used because a considerable

optical loss was caused with a double-pass on several optical interfaces of the Plexiglas/thin pane walls of the expansion cavity. This lowered sensitivity of the ISD method. Also baseline of ISD records was very fluctuant from convex to concave shape due to its variable optical characteristics.

The ISD data were recorded each 0.15 s, and than filtered by moving average over 5 subsequent records in order to reduce signal noise and smooth the shape of baseline. For this purpose the IIR (Infinite Impulse Response) function in LabView was employed. Filtered data were further fitted by Voigt profile using the developed Origin script, which combined Origin Peak fitting module with fixed parameter *wL* and following expressions

$$T = \left(\frac{wG}{14.49} \right)^2 \quad , \tag{1}$$

$$wL = \frac{296}{T \cdot p \cdot \gamma_m} \tag{2}$$

which relate the Lorenztian and Gaussian width. Here T is the temperature to be evaluated, p is the measured cavity pressure, and γ_m is the $I^2P_{1/2} - I_2(^2P_{3/2})$ broadening coefficient for the gas mixture. The iterative procedure was as follows. After an initial guess of wL, T was calculated from the Voigt fit of the peak curve. Using this T value, a new wL was calculated from (2). Using the previous initial and present wL values, a new guess of *wL* was calculated by the bisection method. The iterations were terminated when the two subsequent either *wL* or *wG* values differed less than 0.01%. Finally the Iodine number density from peak area and the temperature from *wG* in the cavity were calculated.

4. Experimental results on the DAIG device

4.1. Cold flow measurements

The cold flow tests of the DAIG device were performed to prove a proper designing of the device nozzle and supersonic cavity. The primary gas was mixed of He and N_2 substituting oxygen flow from SOG. The secondary gas flow was mixed of He (used later as a carrier gas of iodine compound) and Ar substituting the iodine donor. The contribution of the Ar flow rate of 1 mmol/s to the injector pressure corresponds to a molar flow rate of $(40/142)^{0.5} = 0.53$ mmol/s of CH_3I.

The average Mach number, M_P, evaluated from measuring the static pressure by the Pitot tube, p_{st}, and stagnation pressure in the subsonic duct, p_o, was calculated using the formula [18]

$$p_{st} = p_0 \left(1 + \frac{\kappa - 1}{2} M_P^{\,2} \right)^{\frac{-\kappa}{\kappa - 1}}, \tag{3}$$

where κ is the adiabatic constant. The local Mach number M_{loc} was measured at a tip of the Pitot tube, in the center of the cavity, and was evaluated using the formula

$$\frac{P_{pit}}{p_{st}} = \frac{\left(0.5(\kappa+1)M^2\right)^{\frac{\kappa}{\kappa-1}}}{\left(2\frac{\kappa}{\kappa+1}M^2 - \frac{\kappa-1}{\kappa+1}\right)^{\frac{1}{\kappa-1}}}. \tag{4}$$

Three positions of the Pitot tube tip were tested, 56 mm, 80 mm, and 150 mm from the nozzle throat.

A penetration depth of the secondary flow into the primary flow is roughly proportional to the square root of dynamic pressure ratio. The dynamic pressure of the secondary stream is equal to $\rho u^2 = \rho c^2 = \kappa^{0.5} p$ since the flow is sonic at the injector holes. At the sonic condition, pressure is proportional to $n*W^{0.5}$. The qualitative penetration parameter was therefore related to 1 mmol/s of pure argon

$$\Gamma = \sqrt{\frac{\dot{n}_{\mathrm{sec}} W_{\mathrm{sec}}^{0.5}}{\dot{n}_0 W_{Ar}^{0.5}}}, \qquad (5)$$

where P_{pit} is the stagnation pressure measured by the Pitot tube. Three positions of the Pitot tube tip were tested, 56 mm, 80 mm, and 150 mm from the nozzle throat.

The flow situation in the cavity by evaluating the Mach numbers and penetration parameter was studied step by step: *i)* with the primary flow only at different N_2 flow rates, He/N_2 mixture flow rates, and Pitot tube positions, and *ii)* with injection of the secondary gas at different flow rates and two positions of Pitot tube.

Detailed results of these measurements are presented in the report of this grant [17]. Here is given a brief summary of them.

Ad *i)* Measurement with the primary flow

According to the local Mach number, the flow in the cavity center was in the whole range of He flow rate (21–61 mmol/s) subsonic, only the average Mach number indicates slightly supersonic flow (M_p = 1.06).

In measurements with N_2 flow, the flow in the cavity center was supersonic in the whole range of N_2 flow rate (20–35 mmol/s), and the Mach number M_{loc} increased from 2.02 to 2.22 with increasing gas flow. The flow was supersonic at both Pitot tube positions (56 mm and 140 mm from the nozzle throat).

In measurements with He+N_2 mixture at different ratio, both Mach numbers, M_p and M_{loc}, increased with increasing nitrogen flow rate, approaching nearly the value M = 2. The Mach number was also evaluated for three positions of Pitot tube (56, 80, and 150 mm from the nozzle throat). The M_P decreased along the flow due to shock waves in the system (the flow was under-expanded), otherwise the M_{loc} increased as mixing of two parallel streams was achieved.

An effect of the flow choking on the Mach number by means of the butterfly valve placed in the vacuum line was examined. This effect on the pressures in some device locations and M is shown in **Fig. 4.** At 20° choking, the static pressure and spiral trap pressure approached the same value, and the flow began subsonic. The choking did not influence the plenum pressure upstream the nozzle. In similar measurements performed with pure N_2 in the primary flow, the supersonic flow was attained up to 5° choking.

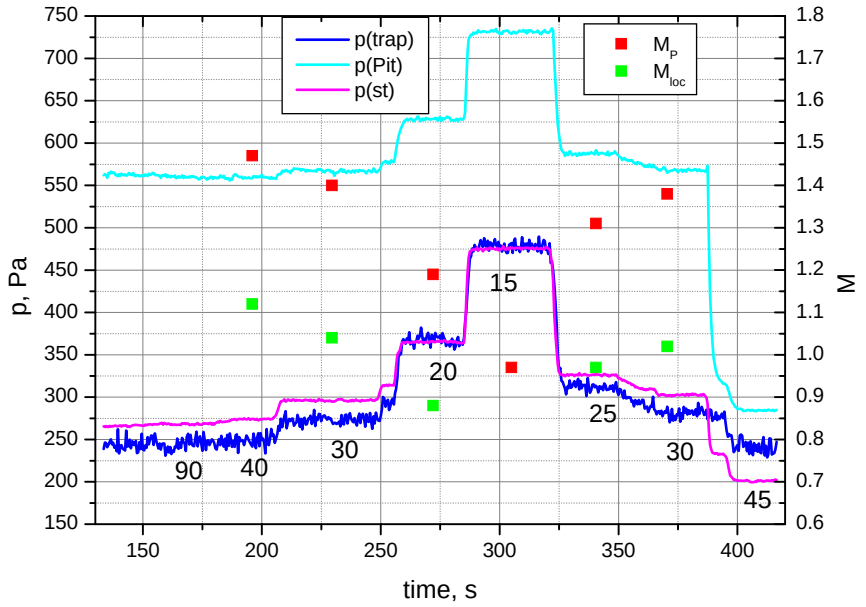

Fig. 4. Effect of gas flow choking by the butterfly valve (numbers denote a choking angle in deg). Experimental conditions: 48 mmol/s He + 21 mmol/s N_2; plenum pressure 913 Pa; Pitot tube distance from throat x = 80 mm

A pressure drop on the two-stage iodine spiral trap was measured with the primary flow of 26 mmol/s He and 26 mmol/s N_2. It was from 173 Pa through 142 Pa to 109 Pa.

Ad *ii)* Measurement with injection of the secondary flow

The secondary flow of only He, only Ar or their mixtures was injected to the primary flow of different composition. The injector with parameters given in Tab. 1 was used, having 15 holes on each side.

The results of these measurements showed that He_{sec} substantially influenced the primary flow. The Mach number was only slightly decreased with Ar flow only but in a mixture with helium M slightly increased with increasing Ar content due to the aerodynamic choking of the primary flow. This was confirmed by increased plenum pressure. The flow was supersonic, the values of both M_P and M_{loc} were in the range of 1.30 – 1.79 evaluated for the Pitot measurements at 80 mm and 150 mm distance from the throat.

With Ar only in the secondary flow and low primary flow rate, the flow was subsonic in the cavity center. With He_{sec} and Ar in the secondary flow, the flow remained still supersonic but M was very low. The static pressure was higher at x = 150 mm than at x = 56 mm, which means that the injection of the secondary flow caused a downstream flow deceleration.

Representative results of these experiments are given in **Table 4.**

Tab. 4
Flow parameters at different secondary flow rates.

x_{Pit}	He_{pr}	N_2	He_{sec}	Ar	p_{st}	P_0	M_P	M_{loc}	Γ
80	23	11	0	1.0	124	491	1.51	subsonic	1.00
80	38	16	0	4.0	189	702	1.46	1.29	2.00
80	42	18	0	4.3	215	787	1.49	1.29	2.08
80	53	14	16	1.1	359	1015	1.26	1.08	2.60
80	54	14	13	2.2	347	1000	1.28	1.08	2.71
80	35	20	16	0.0	322	985	1.35	1.06	3.09
150	36	30	0	2.1	215	683	1.60	1.39	1.45
56	29	32	17	2.6	215	703	1.59	1.42	3.04

4.2. Discharge generation of atomic iodine

Most of experiments were performed under subsonic flow conditions due to two reasons. First, atomic iodine concentrations were too low and ISD signal was too noisy at low supersonic pressures. Second, I_2 trapping in the condensers was much more efficient at higher pressure. Therefore, the pressure in the cavity was 4-5 times increased by a gas flow choking in comparison with a free (non-choked) flow by means of the butterfly valve on the vacuum line. A non-linear shape of the baseline of ISD records complicated the evaluation procedure, resulting in a large scatter of temperature values calculated from these records. An example of the absorption peak corresponding to the atomic iodine number density 1.07 x 10^{14} cm^{-3}, and the temperature of 275 K is shown in **Fig. 5**.

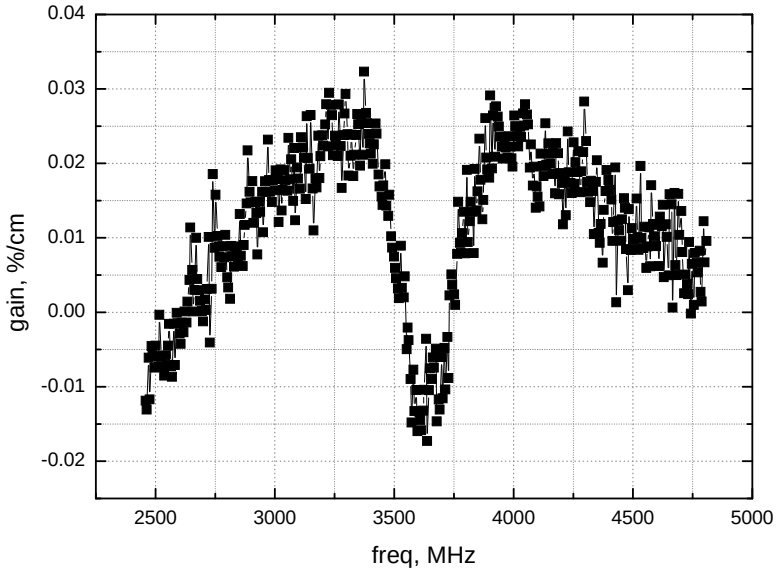

Fig. 5. Absorption peak of atomic iodine. Averaged of 5 subsequent peaks.
p_{cav} = 502 Pa, P_{abs} = 149 W. Flow rates (mmol/s): 0.2 CH_3I; 1.96 Ar; 1.98 He; 20.3 N_2.

4.2.1. Experimental results with CH_3I and their discussion

The secondary gas flowing into the injector/discharge chamber was composed of CH_3I, Ar and He in a ratio 1–3.7 : 10 : 10. This mixture was used in all experiments except of some small variations in Ar and He flow rates. The discharge dissociation measurements were performed in the following conditions: RF power 50–250 W, flow rate of CH_3I 0.1–0.77 mmol/s, Ar 1–3.1 mmol/s, He 0–6 mmol/s, the primary gas flow N_2 10–37 mmol/s, and the cavity pressure 140–850 Pa (~1–10 Torr). The pressure inside the injector (discharge chamber) varied between 2.0 and 3.2 kPa (~15–24 Torr).

An example of the profile record of atomic I number density measured across the cavity at three different distances from the nozzle throat is shown in **Fig. 6**.

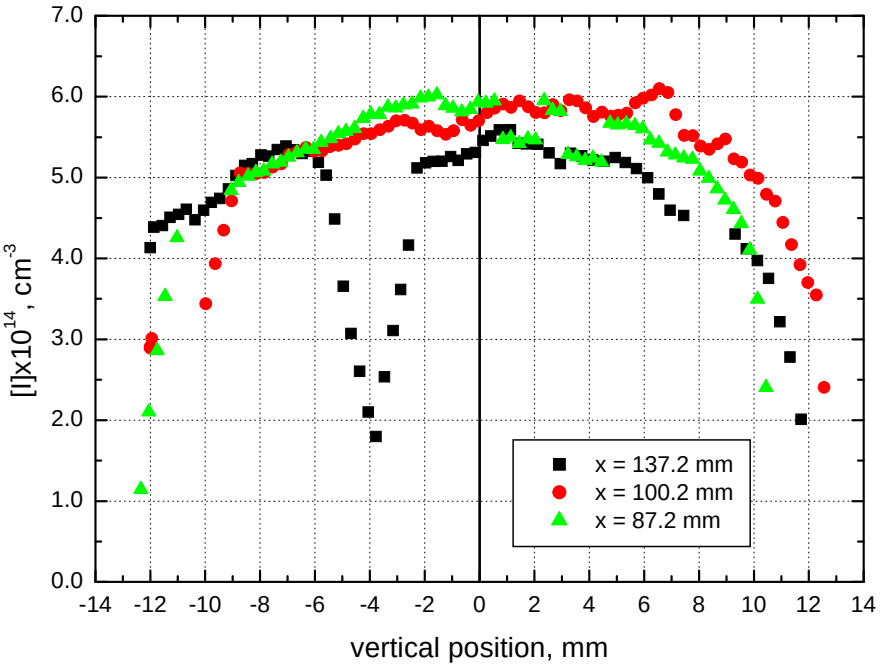

Fig. 6. Vertical profile of I number density at three positions downstream the nozzle throat. p_{cav} 802 Pa, P_{abs} 196 W. Flow rates (mmol/s): 0.74 CH_3I; 2.05 Ar, 1.93 He, 20.4 N_2.

A homogeneous and relatively flat profile was typical for these subsonic-flow measurements. The peak on the black curves was probably due to a discharge spark effect, and such peaks were apparent also to temperature profiles in **Fig. 7**.

The profiles of atomic I density had different character if they were recorded in the cavity with supersonic flow (M = 1.91). This is illustrated in **Fig. 8** for recording in two distances from the nozzle throat. The profiles have more sharp shape but are less homogenous. The temperature is significantly lower than the in the subsonic flow (**Fig. 9**). A transition from the subsonic flow to the supersonic flow was studied by stepwise opening the choking butterfly valve during one

experimental run. The resulting concentration profiles at four different pressures are shown in **Fig. 10**.

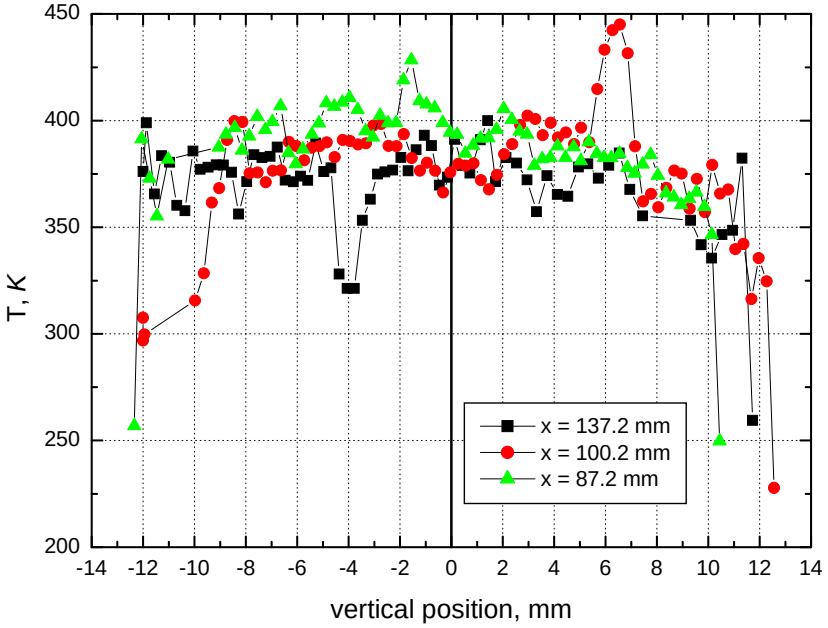

Fig. 7. Vertical profile of temperature at three positions downstream the nozzle throat. Conditions as in Fig.6.

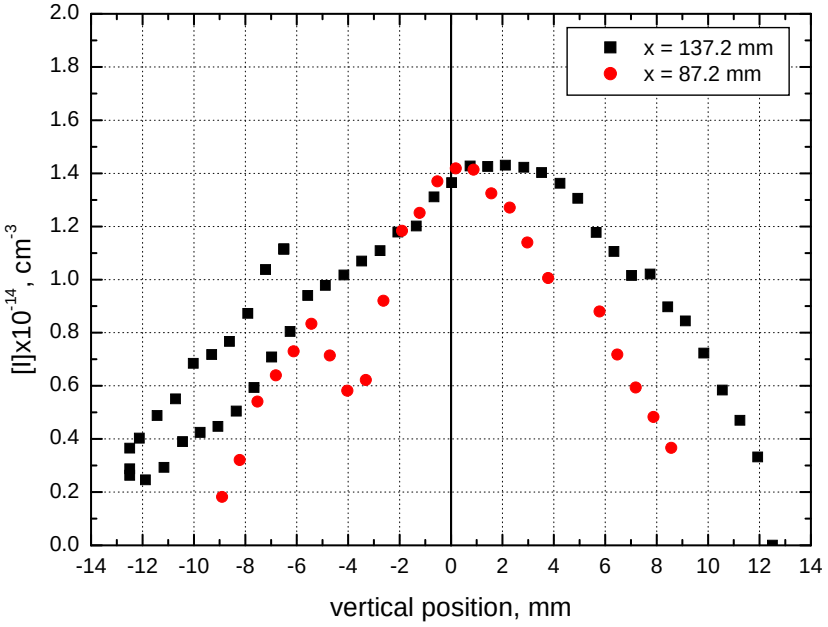

Fig. 8. Vertical profile of I number density at two positions downstream the nozzle throat for the supersonic flow. p_{cav} = 139 Pa, P_{abs} = 250 W. Flow rates (mmol/s): 0.76 CH_3I; 1.95 Ar; 1.92 He; 37.7 N_2.

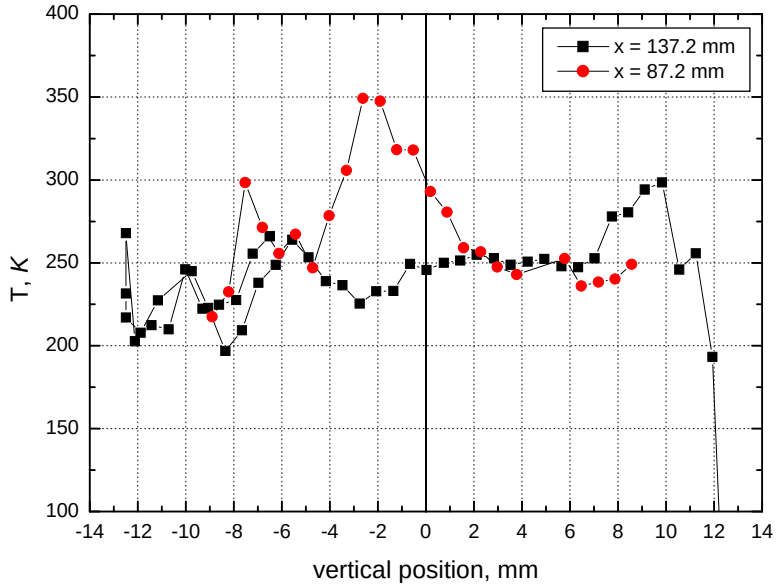

Fig. 9. Vertical profile of temperature at two positions downstream the nozzle throat for supersonic flow. Conditions as is in Fig. 8.

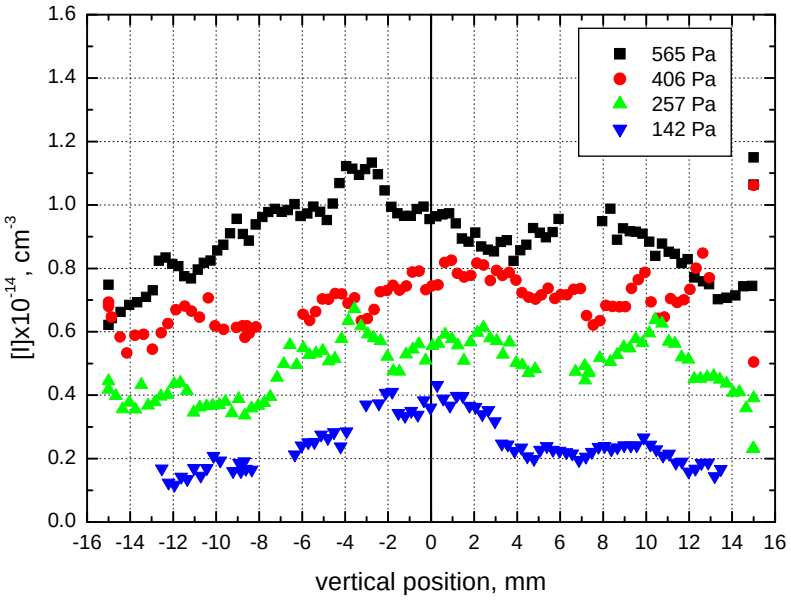

Fig. 10. Vertical profile of I number density at four cavity pressures.
P_{abs} = 52 W; flow rates (mmol/s): 0.53 CH_3I; 1.62 Ar; 2.07 He; 9.8 N_2

The homogenous distribution of I number density was not changed very much with decrease in pressure. This character in contradiction to sharp profiles in Fig. 8 results from much lower N_2 flow rate (9.8 mmol/s *vs.* 37.7 mmol/s). A "double peaks" of the hot jets injected from the RF discharge chamber for lower pressure are seen in **Fig. 11**. The Mach number evaluated for this low pressure of 142 Pa was M = 1.18, whereas other curves corresponded to the subsonic flow (by pressure measured by the Pitot tube located in this experiment 188.2 mm downstream from the nozzle throat in this experiment). It seems that the low primary flow in these experiments was choked rather by the secondary jet (an aerodynamic throat) than by the hardware nozzle throat itself. The concentration profiles measured for five different values of absorbed RF power are shown in **Fig. 12**. A shape of these profiles was not changed with the RF power, and I number densities increased monotonically with increasing power.

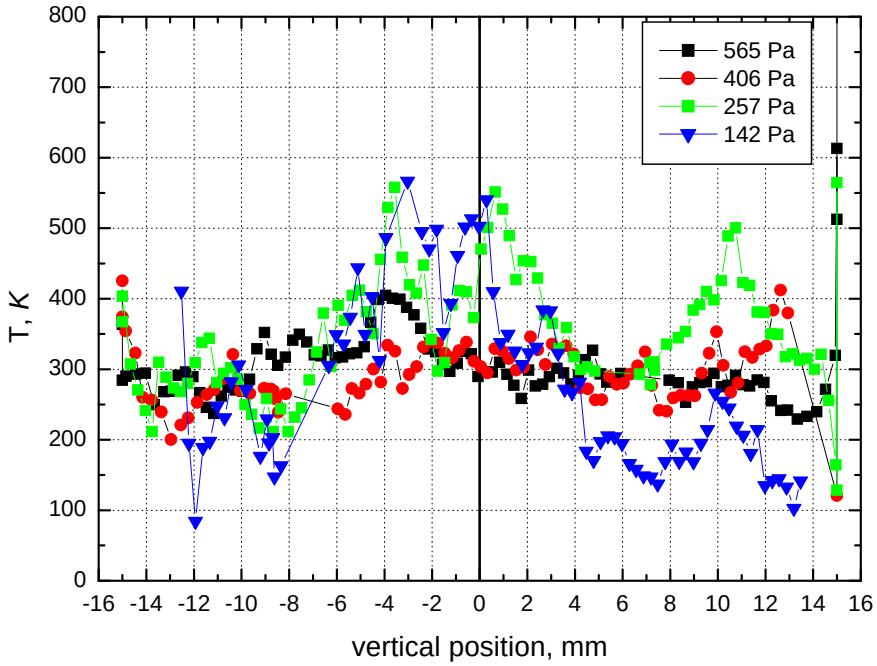

Fig. 11. Vertical profile of I number density at four cavity pressures. Conditions as in Fig. 10

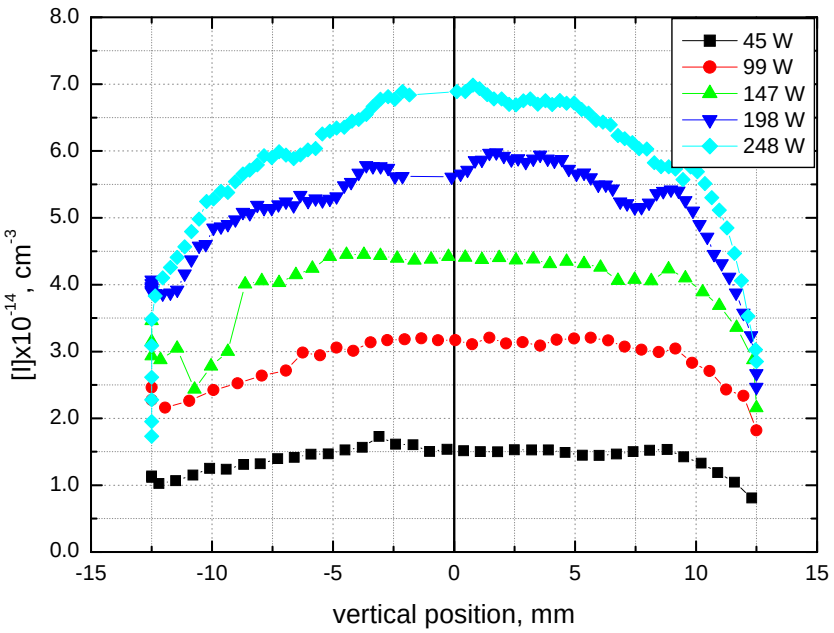

Fig. 12. Vertical profile of I number density at five values of absorbed RF power. p_{cav} = 780 Pa; flow rates (mmol/s): 0.73 CH_3I;1.96 Ar; 1.92 He; 20.6 N_2

A dissociation fraction of CH_3I was evaluated in a following manner. First, an average partial pressure of atomic iodine in the cavity was calculated according to

$$p_I = \frac{1}{|y_{up}| - |y_{bott}|} N_A \int_{y_{bott}}^{y_{up}} c_I(y) RT(y) dy, \qquad (6)$$

where $c_I(y)$, $T(y)$ are evaluated number density and temperature profiles. Then the dissociation fraction is

$$\eta_{diss} = \frac{p_I}{p_{cav}} \frac{\dot{n}}{\dot{n}_{CH3I}} \times 100 \quad \%\,.\,, \qquad (7)$$

where $\dot{n} = \dot{n}_{Ar} + \dot{n}_{He} + \dot{n}_{N2} + \dot{n}_{CH3I}$ is the total gas flow rate.

The η_{diss} ranged from 2.8% at 0.2 mmol/s CH_3I and RF power 49 W to 17.6% at 0.74 mmol/s CH_3I and 247 W. It was observed that the dissociation fraction was relatively insensitive to variation of Ar flow rate in the range of 1.9 – 2.9 mmol/s Ar at the constant He flow rate. The He flow rate increase above 2 mmol/s at the Ar flow rates 1.9 mmol/s or 2.9 mmol/s developed a slight negative effect on the dissociation degree.

The dependence of η_{diss} on the absorbed RF power for four values of CH_3I flow rate is shown in **Fig. 13.** The dissociation fraction increased linearly with the RF power, and decreased with

increasing CH_3I flow rate. The corresponding dependences of the average I number density and the average temperature (averaged across the cavity height) are shown in **Figs. 14** and **15**.

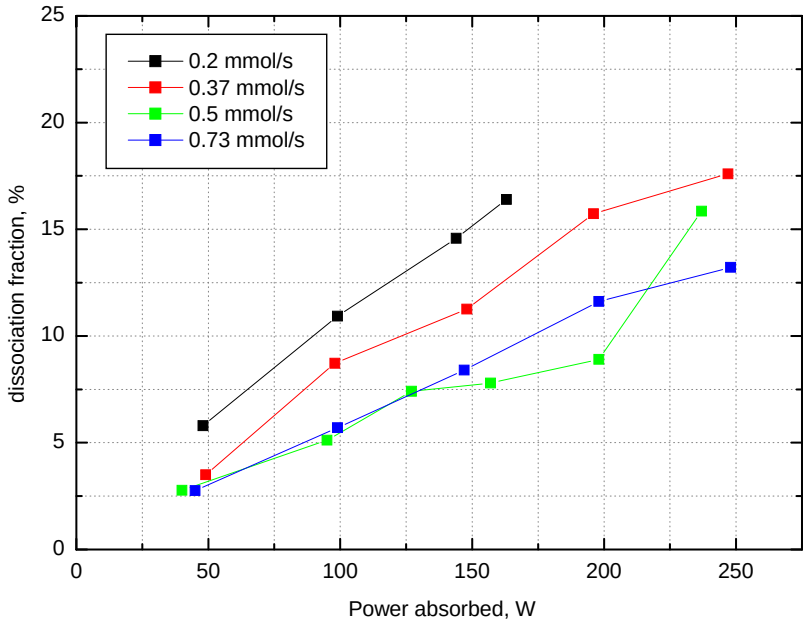

Fig. 13. Dependence of CH_3I dissociation fraction on the absorbed RF power. p_{cav} = 560-780 Pa; flow rates (mmol/s): 1.9 Ar; 1.9 He; 10–20 N_2

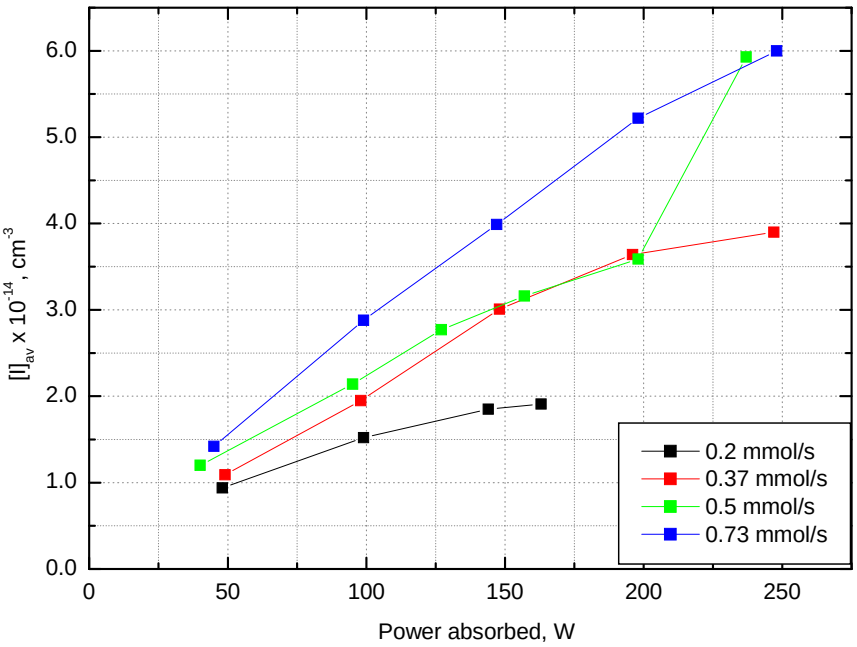

Fig. 14. Dependence of average I number density on absorbed RF power. CH_3I, conditions as in Fig. 13.

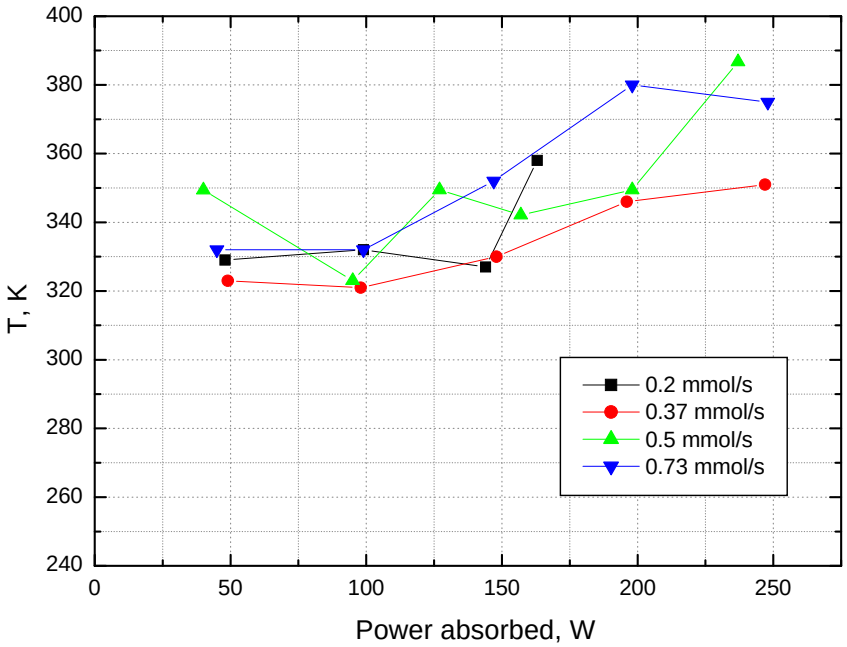

Fig. 15. Dependence of average temperature on absorbed RF power. CH_3I, conditions as in Fig. 13.

4.2.2. Experimental results with CF_3I and their discussion

Experiments with CF_3I were performed recently in a few experimental runs and at lesser extent of experimental conditions than experiments with CH_3I due to a terminated research period and also a smaller amount of CF_3I at our disposal that time. The experiments were performed under following experimental conditions: RF power 50-200 W, flow rates of 0.18–0.91 mmol/s CF_3I, 2–4.9 mmol/s Ar, 0–2 mmol/s He, and 20 mmol/s N_2, and the cavity pressure 520–680 Pa (~3.8–5.1 Torr). The pressure in the injector varied between 2.2 and 4.6 kPa (~16.5 – 34 Torr).

There was no significant difference in the profile shapes of I number density between both investigated alkyl iodides. The dependence of atomic iodine concentration on the absorbed RF power is shown in **Fig. 16**, and the dependence of dissociation fraction on the absorbed RF power for four different CF_3I flow rates in **Fig. 17**. Also the dissociation fraction, η_{diss}, measured for CF_3I at similar conditions was very close to the values for CH_3I. The dashed lines in Fig. 17 were measured with Ar only used as a buffer gas, which was substantially better than with Ar + He mixture in the ratio 1 : 1. A possible explanation of this fact could be a higher content of the excited states and ions in the discharge medium, which might increase the rate of photodissociation and electron-impact dissociation of CF_3I. The highest value of dissociation fraction was 22.5% for the flow rate of CF_3I 0.2 mmol/s. This was about 1.6 times higher than for the same flow rate of CH_3I.

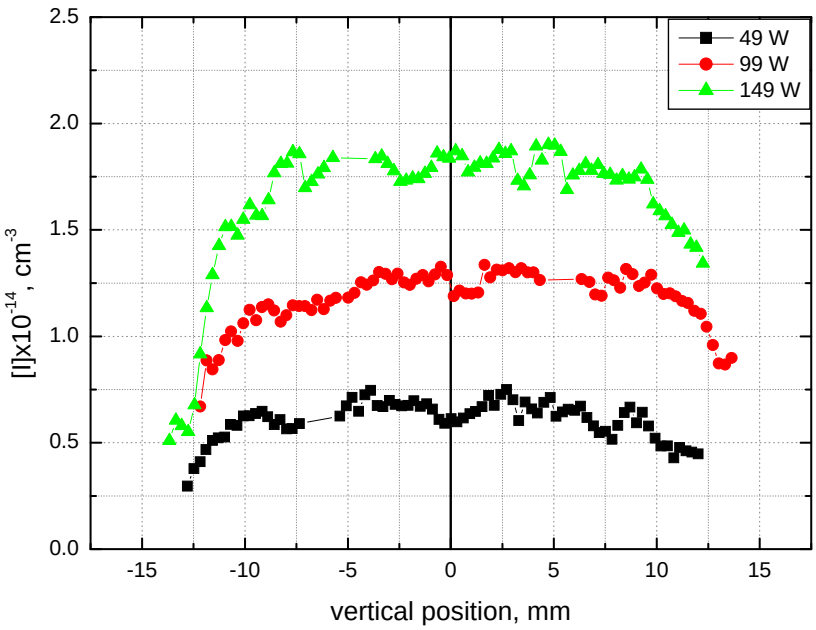

Fig. 16. Vertical profile of I number density at three values of absorbed RF power. p_{cav} = 510 Pa; flow rates (mmol/s): 0.35 CF_3I; 1.96 Ar; 2.04 He; 20.5 N_2

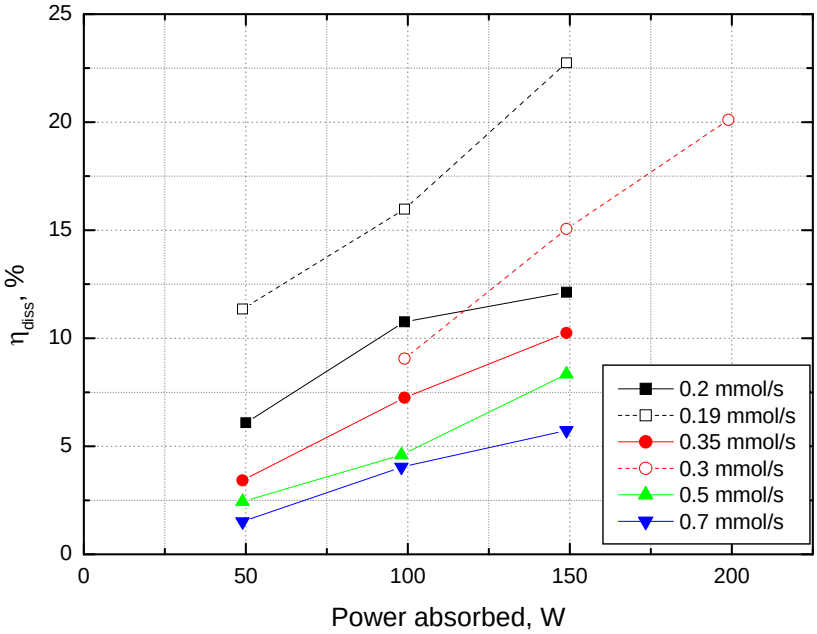

Fig. 17. Dependence of CF_3I dissociation fraction on absorbed RF power. p_{cav} = 500 Pa; f low rates (mmol/s): 1.9 Ar (solid lines) or 3.1 (dashed line); 1.9 He (solid) or 0 He (dashed); 10-20 N_2

Corresponding dependences of the average I number density and average temperature (averaged across the cavity height) are shown in **Figs. 18** and **19**. Both these parameters are lower in comparison with analogous dependences for CH_3I (Figs. 14 and 15), but the reason for this could be in the fact that the dependence for CF_3I was measured at lower pressure (500 Pa) than for CH_3I (800 Pa). It can be however seen that the dependencies of dissociation fraction on the absorbed RF power for both CF_3I and CH_3I are increasing in the studied power range; otherwise the dissociation fraction did not reached a point of saturation yet, which is very promising for the next improvement.

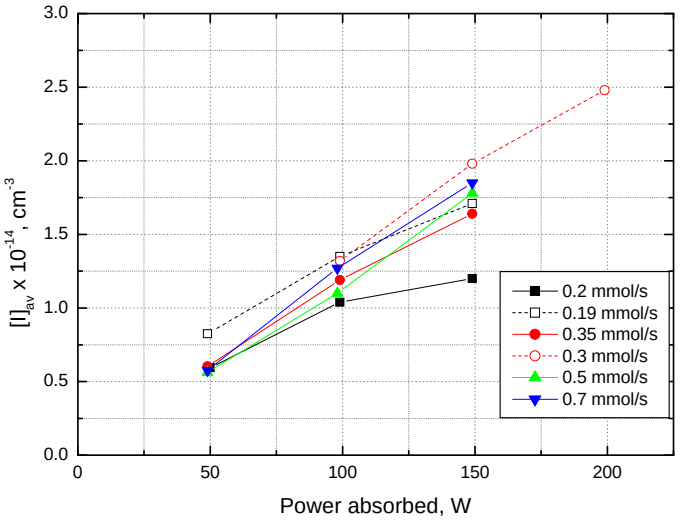

Fig. 18. Dependence of average I number density on RF absorbed power. CF_3I, conditions as in Fig. 17.

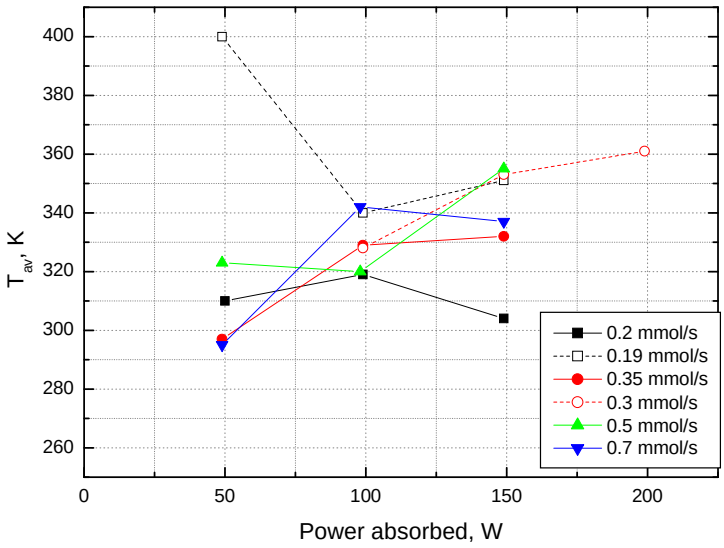

Fig. 19. Dependence of average temperature on absorbed RF power. CF_3I, conditions as in Fig. 17

4.2.3. Energy balance

The following energetic parameters were evaluated:

i) the energy needed to generate one iodine atom (or to dissociate one iodine donor molecule)

$$E_{diss} = \frac{E_{abs}}{N_I} = \frac{P_{abs}}{e\dot{N}_I} \quad \text{[eV / atom]}, \tag{8}$$

where P_{abs} is the absorbed RF power in W, $\dot{N}_I = \frac{p_I \dot{n}}{p_{cav}} N_A$ is the number of I atoms per second, and e is the electron charge,

ii) the fraction of power going to the dissociation

$$fP_{diss} = \frac{P_{diss}}{P_{abs}} = \frac{e\dot{N}_I E_{bond}}{P_{abs}} = \frac{E_{bond}}{E_{diss}}, \tag{9}$$

where E_{bond} is the dissociation energy of C-I bond (2.47 eV/molec for CH_3I, and 2.34 eV/molec for CF_3I),

iii) the fraction of RF power going to heat

$$fP_{heat} = \frac{P_{heat}}{P_{abs}} = \frac{\dot{n}_{mix} c_{pmix} T - \dot{n}_1 c_{p1} T_0 - \dot{n}_2 c_{p2} T_0}{P_{abs}}, \tag{10}$$

where the products $\dot{n} c_p T$ represent the enthalpy per second of the mixed primary and secondary flow, T is the temperature evaluated from the ISD measurement and T_0 is 293 K. A remaining part of the absorbed power, $fP_{lost} = 1 - fP_{diss} - fP_{heat}$, was either removed by the injector water-cooling or converted to some excited states of the discharge species.

Values of the above defined parameters for selected experiments with CH_3I and CF_3I are given in **Table 5.**

Tab. 5

Energetic parameters for selected experiments
P_F - the input RF power; P_B - reflected RF power; absorbed RF power $P_{abs} = P_F - P_B$.
V_{DC} - DC voltage offset measured by RF source. Flow rates: 2 mmol/s Ar, 2 mmol/s He, RF frequency 40 MHz

I donor	n_{donor} mmol/s	n_{N2} mmol/s	P_{cav} Pa	P_{inj} kPa	P_F W	P_B W	P_{abs} W	V_{DC} V	E_{diss} eV/at	η_{diss} %	fP_{diss} %	fP_{heat} %	fP_{lost} %
CH_3I	0.25	20.8	744	2.09	50	2	48	-6	34.2	5.8	7.2	51.8	41.0
CH_3I	0.20	20.8	733	2.49	150	6	144	-150	52.6	14.6	4.7	16.3	79.0
CH_3I	0.51	10.7	527	2.49	100	5	95	-30	37.7	5.12	6.6	12.6	80.8
CF_3I	0.20	20.3	494	2.46	150	1	149	-130	63.1	12.1	3.7	5.0	91.2
CF_3I	0.35	20.4	553	2.50	150	1	149	-94	43.1	10.2	5.4	17.9	76.0
CF_3I	0.49	20.7	541	2.29	50	1	49	-64	42.3	2.44	5.5	42.8	51.7

The dependence of the fraction fP_{diss} on the absorbed power going into the dissociation for different CH_3I flow rate is shown in **Fig. 20** and in **Fig. 21** for CF_3I. The fP_{diss} values generally slightly decreased with increasing RF power. In the case of CH_3I, this parameter mostly increased with increasing the iodide flow rate, while for CF_3I it was nearly independent on its flow rate.

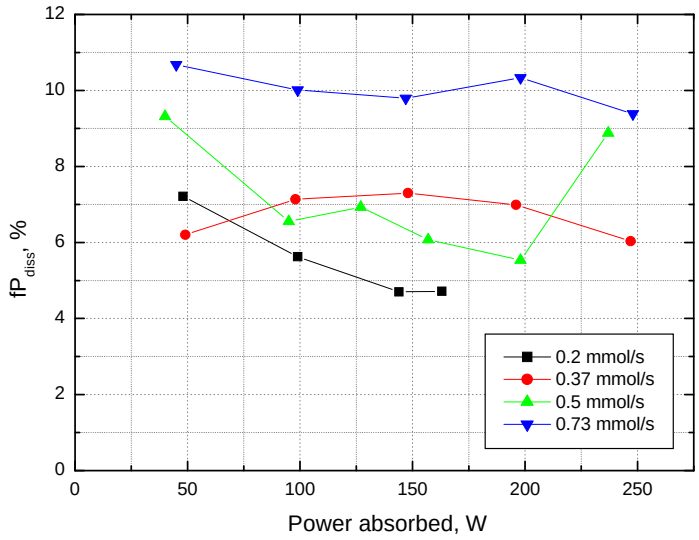

Fig. 20. Dependence of fraction of absorbed RF power going into CH_3I dissociation on total absorbed RF power.
p_{cav} = 560-780 Pa; flow rates (mmol/s): 1.9 Ar; 1.9 He; 10–20 N_2 (conditions as in Fig. 13)

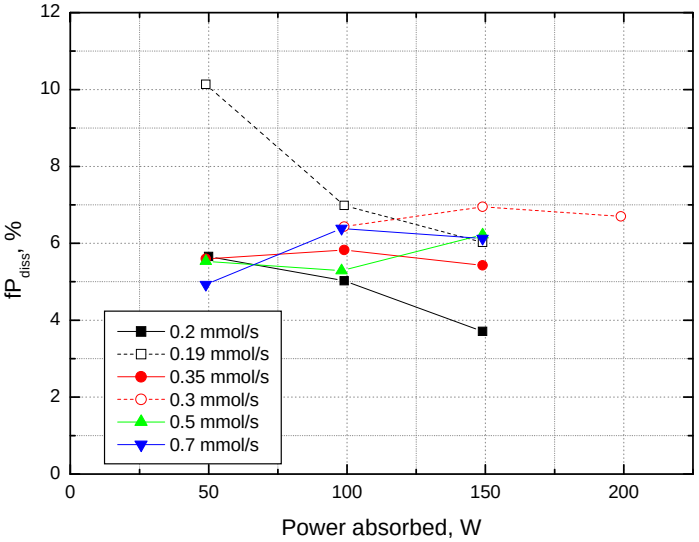

Fig. 21. Dependence of fraction of absorbed RF power going into CF_3I dissociation on absorbed RF power.
p_{cav} = 500 Pa; f low rates (mmol/s): 1.9 Ar (solid lines) or 3.1 (dashed line);
1.9 He (solid) or 0 He (dashed); 10-20 N_2 (conditions as in Fig. 17).

The dependence of the fraction on the absorbed the absorbed RF power going into heat for different iodide flow rate is shown in **Fig. 22** for CH_3I and **Fig. 23** for CF_3I. Very high values of fP_{heat} were obtained for 50 W of absorbed power with CH_3I for all flow rates contrary to data at higher RF powers. This effect was not measured for CF_3I.

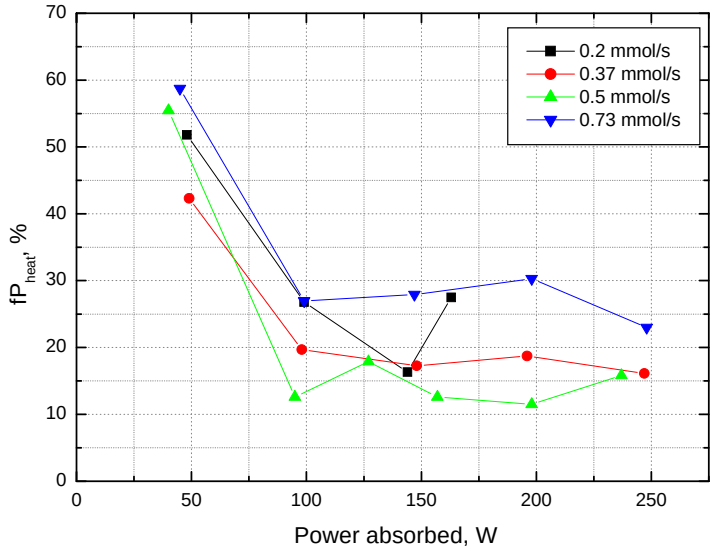

Fig. 22. Dependence of fraction of absorbed RF power going to heat on absorbed RF power. CH_3I, p_{cav} = 560-780 Pa; flow rates (mmol/s): 1.9 Ar; 1.9 He; 10–20 N_2 (conditions as in Fig. 13)

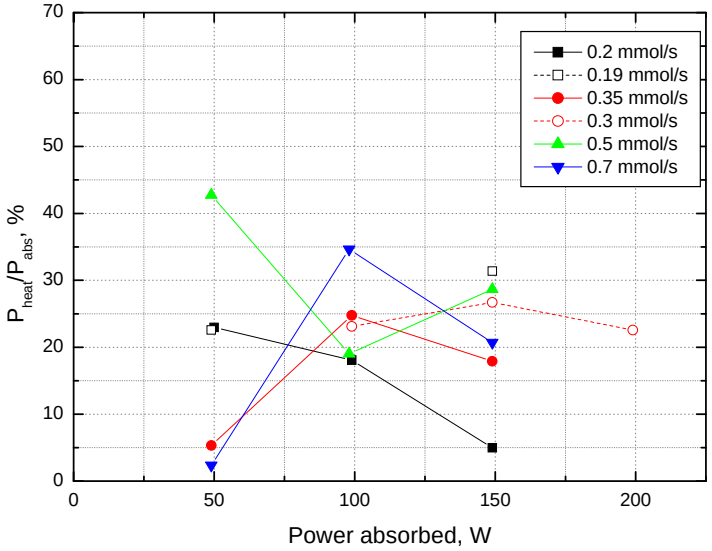

Fig. 23. Dependence of fraction of absorbed RF power going to heat on absorbed RF power. CH_3I, p_{cav} = 560-780 Pa; flow rates (mmol/s): 1.9 Ar; 1.9 He; 10–20 N_2 (conditions as in Fig. 13)

4.2.4. Homogeneous recombination of atomic iodine

The value of the dissociation fraction measured in the cavity at some distance from the injector exit can differ from values of atomic iodine concentration exiting the discharge owing to the recombination processes, for example

$$X + I + M \rightarrow XI + M \qquad X = CH_3, CF_3 \qquad (11)$$

The value of the rate constant found in literature for the ternary reaction of CF_3 radical is $k_3(CF_3)$ = 1.3 x 10^{-28} cm^6s^{-1} [20], and the rate constant of two-body reaction (high-pressure limit) is $k_2(CF_3)$ = 1.54 - 2.15 x 10^{-11} cm^3s^{-1} at 300 K [21]. As for CH_3I, only two-body constant was found, $k_2(CH_3)$ = 9.96 x 10^{-12} cm^3s^{-1} at 298 K [22].

In few experiments with CH_3I, a dependence of the dissociation fraction on the distance from the nozzle throat, x, was measured. It was found that η_{diss} slightly decreased with increasing this distance, e.g. from 11.8% at x = 87.9 mm to 10.1% at x = 137.2 mm. This measurement was performed at the flow rates: 0.74 mmol/s CH_3I, 2.05 mmol/s Ar, 1.93 mmol/s He, and 20.4 mmol/s N_2. Taking into account the fact that η_{diss} values were evaluated at both places using the same p_{cav} value, and then the difference between them could be smaller due to a pressure drop downstream. The dissociation fraction was similar in both subsonic and supersonic experiments under the same flow rates. These results showed upon probably very low recombination rate under examined conditions.

The experiments with CF_3I at different positions could not be unfortunately performed by the project termination and also due to small amount of this iodine donor at our disposal that time. By example calculation, the $k_3(CF_3)$ value gives 89% drop of η_{diss} at x = 10 cm distance related to the initial CF_3I concentration of 3 x 10^{14} cm^{-3}. This means that this rate constant $k_3(CF_3)$ does not correspond to conditions of our experiments since all atomic iodine would be already recombined at a detection place. This can be ascribed to the fact that the literature value of $k_3(CF_3)$ was obtained for pressure of one order of magnitude higher than the pressure in our experiments. However, there are three reasons to suppose that the recombination rate is substantially higher for CF_3I than for CH_3I: 1) $k_2(CF_3)$ is 2–3 higher than $k_2(CH_3)$, 2) only very small amount of I_2 was trapped on the condenser walls during experiments with CF_3I in comparison with CH_3I (see Photo 15); and 3) the dissociation fraction decreased with increasing donor flow rate more rapidly for CF_3I than for CH_3I. We can therefore expect substantially higher dissociation fraction for CF_3I at supersonic conditions in the cavity, and for shorter distance x from the nozzle throat.

5. Summary of the grant achievements

The idea of radiofrequency discharge generation of atomic iodine for COIL from appropriate iodine donor compounds directly in the iodine injector was developed into originally designed and constructed device for experimental study of this method. A key part of the device, the joint body of injector, discharge chamber and double slit supersonic nozzle, was designed with a substantial support of the computational modeling of most suitable hydrodynamic and dimensional parameters,

taking into account all three roles of this body. Also other parts of the device were designed on the base of calculation results, e.g. the cooling efficiency of the spiral molecular iodine trap.

The technical design of the whole DAIG device including elaboration of the technical drawings for manufacturing of individual parts was accomplished in our department. The construction of the device was completed, inclusive of gas handling system and gas lines, the RF power connection and impedance matching to the device, water cooling/heating line for iodine injector, installation of the cooler/heat exchanger for molecular iodine trap, trap washing/draining tank. Needed measuring and diagnostic instruments (vacuum pump, flow meters, pressure gauges, RF power source, tunable diode probe laser on moving stage, alkyl iodide management, etc.) were subjoined to the DAIG device. The LabView software was purchased from National Instruments for the data acquisition system, and the special program was developed under this software for experimental data processing by PC on-line.

The comprehensive literature review of characteristics and physical properties of iodine donor compounds potentially considered for experimental investigation was performed, and two alkyl iodides, CH_3I and CF_3I, were purchased for the initial study during the last period.

The CFD modeling of small-signal gain for the DAIG device was accomplished. These calculations proved that the standard Heidner model (H-model) predicted substantial increase in the rate of iodine dissociation in presence of atomic iodine with some degree of I_2 predissociation. This corresponded to a rapid build-up of the small-signal gain but also to a rapid initial decrease in the $O_2(^1\Delta)$ yield. The simulations using the Heidner-Azyazov-Heaven-Lilenfeld dissociation (HLAH-model) provided similar rate of dissociation like the H-model for the 50% predissociation but the ssg values were somewhat lower. Simple estimations of the chemical efficiency from the H-model predicted a relative enhancement of the chemical efficiency up to 24% at 100% predissociation, and up to 15% at 50% predissociation. The HLAH-model predicted much lower enhancement of the chemical efficiency; by 2.7% only for the 50% predissociation. On the whole, our CFD modeling results showed that the COIL performance enhancement by the I_2 (or other atomic iodine donor) predissociation is rather complex task, requiring to take into account a cavity design and injection/mixing scheme, and other kinetic, flow and pressure conditions in the system. Nevertheless, these modeling results were encouraging in getting positive enhancement of the small-signal gain and laser power by our proposed method of iodine donors predissociation by RF discharge on device constructed in our laboratory.

The cold flow measurements were performed to test the designed supersonic cavity with a double slit nozzle and at different flow conditions by evaluation of the Mach number. It was proved that this nozzle with a center iodine injector behaved perfectly with the primary flow of pure N_2, expanding it to the Mach number up to ~2 along the entire cavity. The injection of secondary He/Ar mixture into the primary N_2 flow decreased slightly the Mach number due to helium in the mixture mainly.

The hot flow experiments have been performed, starting with CH_3I as the iodine donor, and then with CF_3I. Using CH_3I, the atomic iodine concentrations up to 7.5×10^{14} cm^{-3} and 1.4×10^{14} cm^{-3} were achieved in subsonic and supersonic flow, respectively. The dissociation fraction increased

linearly with the increasing RF power in the tested range and flow conditions, and it was not evidently saturated yet at loaded RF power. The highest attained value was 17% measured at 250 W of the input RF power and RF frequency 40 MHz. It was proved that a backward recombination of I with CH_3 was fairly slow in studied conditions. Using CF_3I, the atomic iodine concentrations up to 3.2×10^{14} cm^{-3} were achieved in subsonic flow. The dissociation fraction up to 23% was obtained at 200 W of the input RF power and 40 MHz. The dissociation fraction was probably diminished by a backward recombination of I with CF_3, and should be substantially higher at supersonic flow conditions. These experiments were not performed yet by termination of this grant, and due to small amount of CF_3I at our disposal that time. A fraction of the absorbed RF power going to the dissociation was between 3% and 11%, and was a bit better in case of CH_3I. The fraction of absorbed RF power going to heat of the discharge medium was between 7% and 48% in case of CH_3I, and between 2% and 33% in case of CF_3I. Despite of much higher price, CF_3I seems to be more promising candidate for laser experiments than CH_3I. The limited number of supersonic experiments showed that a sufficient Mach number and good homogeneity in both I number density and temperature can be achieved with 2 mmol/s of Ar and 2 mmol/s of He in the secondary flow and $N_2 > 30$ mmol/s in the primary flow.

6. Conclusions and plans for following-on research

The above described experiments realized on the entirely new device constructed from a ground, and gathered first experimental results with two iodine donors during this two-year grant can be considered as a good base for following-on research on this problem in the COIL technology. They provided much experience and information about the studied system, and also revealed issues that need more systematic study and improvements in the device modifications and experimental conditions in order to increase the efficiency of this method of atomic iodine generation (a dissociation degree and atomic iodine number density).

We plan in the following-on research on this subject for example:

- modification of the nozzle throat height to achieve better supersonic flow conditions in the cavity at given flow conditions;
- elimination of the problem of a carbon deposit on the glass insulation of RF electrode from decomposed RI molecules resulting in undesired random surface sparkle at the RF power higher than 200 W by optimization of plasma conditions (by e.g. shortening of the wolfram rod electrode, and more delicate impedance matching)
- testing a periodically pulsed RF mode;
- testing other configurations of injector holes (their diameter, route into the primary flow)
- extending this study to other iodine donor molecules (DI, HI, I_2, C_3F_7I);
- variation of the secondary gas composition inclusive of adding of small amount of N_2, NO or other gases into the discharge.

7. References

[1] V. Jirásek, O. Špalek, J. Kodymová, and M. Čenský, „Chemical generation of atomic iodine for chemical oxygen-iodine laser. I. Modeling of reaction systems, Chem. Phys. **269**, 167 (2001)

[2] O. Špalek, V. Jirásek, M. Čenský, J. Kodymová, I. Jakubec, and G. D. Hager, „Generation of atomic iodine for the chemical oxygen-iodine laser. II. Experimental results., Chem. Phys. **282**, 147 (2002)

[3] O. Špalek, M. Čenský, V. Jirásek, J. Kodymová, I. Jakubec, and G. D. Hager**, "**Chemical oxygen- iodine laser using a new method of atomic iodine generation", IEEE J. Quant. Electron. **40** (5), 564 (2004)

[4] V. Jirásek , O. Špalek, M. Čenský, I. Picková, J. Kodymová, and I. Jakubec, "Generation of atomic iodine via fluorine for chemical oxygen-iodine laser", Chem. Phys. **334**, 167, (2007)

[5] V. Jirásek, M. Čensky, O. Špalek, J. Kodymová, I. Picková, and I. Jakubec, **"**Chemical oxygen-iodine laser with atomic iodine generated via fluorine atoms", Chem. Phys. **345,** 14 (2008)

[6] T. Wakazono, K. Hashimoto, T. Takemoto, T. Uchiyama, and M. Muro, „The study of chemical oxygen-iodine laser using RF discharge dissociation of I_2", Proc. SPIE, Vol. **3574**, 290 (1998)

[7] T. Madden, G. Hager, A. Lampson, and P. Crowell, "A comparison of subsonic and supersonic mixing mechanism for the chemical oxygen-iodine laser (COIL) using computational fluid dynamic (CFD) simulations", Proc. SPIE, Vol. **3612**, 135 (1999)

[8] D. Carroll, and W. Solomon, "ElectriCOIL: An Advanced chemical Iodine laser concep ", Proc. SPIE 4184, 40, 2000

[9] H. Okamoto, T. Hirata, K. Shinoda, S. Takeda, D. Sugimoto, and M. Endo, „Supersonic chemical oxygen-iodine laser with microwave predissociation of iodine", 31st Plasmadynamics and Lasers Conference, 2000, Denver, Colorado, AIAA Paper 2000-**2492**

[10] M. Endo, D. Sugimoto, H. Okamoto, K. Nanri, T. Uchiyama, S. Takeda, and T. Fujioka, "Output power enhancement of a chemical oxygen-iodine laser by predissociated iodine injection", Jpn. J. Appl. Phys. 39, 468 (2000)

[11] P. A. Mikheyev, A. A. Shepelenko, A. I. Voronov, N. V. Kupryaev, „Atomic iodine production in a gas flow by decomposing methyl iodide in a dc glow discharge", Quantum Electronics **32** (1), 1, 2002

[12] N. N. Yuryshev, N. P. Vagin, A. F. Konoshenko, and V. S. Pazyuk, „Pulsed COIL with volume generation of iodine atoms in electric discharge", Proc. SPIE, Vol. **4631**, 271 (2002)

[13] B. Quillen, and W. Schall, „Iodine dissociation with an RF-discharge", CD Proc. of the COIL R&D Workshop, Stuttgart, Germany, Oct. 2003

[14] J. Schmiedberger, and H. Fujii, „RF plasma jet generator of singlet delta oxygen and RF discharge pre-dissociation of iodine for oxygen-iodine laser at lowered temperature", Proc. SPIE, Vol. **5777**, 211 (2004)

[15] Interim Report – Research Phase 1 of this grant # FA8655-06-1-3034, submitted 15 November 2006

[16] Phase Report – Research Phase 1 of this grant # FA8655-06-1-3034, submitted 14 May 2007

[17] Interim Report – Research Phase 2 of this grant # FA8655-06-1-3034, submitted 15 November 2007

[18] M. J. Zucrow, and J. D. Hoffman, Gas dynamics, John Wiley & sons, New York

[19] R. H. Perry, and D.W. Green, Perry's chemical engineering book, 7th edition, McGraw-Hill, New York, 1997
[20] A. M. Velichko, E. B. Gordon, A. A. Nadelkin, A. I. Nikitin, V. L. Tal'roze, "Role of secondary chemical reactions in the multiphoton dissociation of CF_3I", High Energy Chem. **19**, 1985
[21] NIST Kinetic Database, http://kinetics.nist.gov/kinetics/index.jsp
[22] T. F. Hunter, K.S. Kristjansson, "Optoacoustic method of measuring reaction rates of the radicals CH_3, CD_3, C_2H_5 and CH_2I with I and I_2", J. Chem. Soc. Faraday Trans. 2, **78**, 1982

Acknowledgements

The investigators are very grateful to the US AFRL/DED at Kirtland AFB, NM for the financial support of this research via the USAF EOARD Grant.

We wish to thank Dr. Timothy Madden and Dr. Kevin Hewett at the US AFRL/DED for beneficial discussions on the grant tasks and encouragement.

We thank Dr. A. Gavrielides, Program Manager Lasers and Electro-Optics, Mrs. Susan Fuller, Contract Officer, and Mrs. Jeannette Cyrus, Program Analyst at the USAF EAORD for their very helpful assistance with the Grant processing.